Remotely sensing primary production recovery following bushfire

by

Ivan Kotzur

Submitted in partial fulfilment of the requirements for the degree of
Bachelor of Science with Honours
in the Fenner School of Environment and Society,
Australian National University
October 2018

Australian
National
University

Candidate's Declaration

This thesis contains no material which has been accepted for the award of any other degree or diploma in any university. To the best of the author's knowledge, it contains no material previously published or written by another person, except where due reference is made in the text.

Ivan Kotzur Date:

Acknowledgements

Thanks to Marta Yebra for giving me your time, making connections and assisting me throughout. Thanks also to Randall Donohue at CSIRO for allowing me to come running around the place, and for always getting back to me on (very little) time. Siyuan Tian was a keen eye when I needed one. To Michael Hutchinson and Ian Marang for access to and assistance with the ANU Climate v2 data. Thanks to Lachlan for an endless supply of Bushells bags and to Ellis for occasionally showing up for lunch. Thanks to Eve, Gabriel, Jess and Jason for keeping me focused.

Land of the Yuin nation of South Coast, Australia (Deua-NP).

Abstract

Vegetation growth is the key process driving landscape dynamics and carbon flux. Fire disturbs gross primary productivity to varying degrees depending on fire effects and the ability of the landscape to absorb these. Simple remote sensing diagnosis can build a description of vegetation growth considering physiological drivers from the top down, which are related to fire disturbance through time. Analysis of these disturbances in terms of ecosystem processes at landscape scales are not common. This method used here produces results showing a near constant relationship between fire severity and vegetation type, and time to GPP recovery in a semi-arid shrub landscape. Other landscapes with structurally complex vegetation show a range of GPP values and recovery trajectories with time after fire. The balance of radiation and conductance model components' response to fire disturbance needs to be analysed further. The work here highlights the opportunities in remote sensing available to analysis of landscape disturbance and the potential for integrating such fluctuation into landscape models.

Table of Contents

List of Figures

List of Tables

List of Equations

List of acronyms and abbreviations

ACT – Australian Capital Territory

ANU – Australian National University

CASA – Carnegie Ames Stanford Approach

CRS – Coordinate Reference System

EBF – Evergreen Broadleaf Forest

ENF – Evergreen Needleleaf Forest

ET – Evapotranspiration

ESA – European Space Agency

GPP – Gross Primary Productivity

GDAL – Geospatial Data Abstraction Library

IGBP – International Geosphere-Biosphere Program

FLUXNET– global network of micrometeorological tower sites

GVMI – Global Vegetation Moisture Index

HDF – Hierarchical Data Format

JULES – Joint UK Environment Simulation

JMP – title of SAS statistical software

LAI – Leaf Area Index

LUE – Light Use Efficiency

LPDAAC – Land Processes Distributed Active Archive Center

MODIS – Moderate Resolution Imaging Spectroradiometer

NP – National Park

NBR – Normalised Burn Ratio

NDVI – Normalised Difference Vegetation Index

NCI – National Computational Infrastructure

NSW – New South Wales

NPP – Net Primary Productivity

NVIS – National Vegetation Information System

NIR – Near Infrared

OSH – Open Shrubland

PM – Penman-Monteith

PFT – Plant Functional Types

PAR – Photosynthetically Active Radiation

rdNBR – relativised differenced Normalised Burn Ratio

RS – Remote Sensing/Remotely Sensed

RMI – Residual Moisture Index

SWIR – Short Wave Infrared

SE – South-East

TMP – Terrestrial Biosphere Model

USGS – United States Geological Survey

VI – Vegetation Indice

VPD – Vapour Pressure Deficit

WUE – Water Use Efficiency

Chapter 1: Introduction

Bushfires are a major force of change in many landscapes and for all creatures, including humans. They recycle the work of much productive behaviour. Gross primary production (GPP) is the driving force of living organisms on earth. It is also the largest global flux of carbon dioxide (CO_2), absorbing quantities from the atmosphere (Beer et al., 2010). This process is of absolute importance to life with anthropogenic carbon emissions increasing concentrations to an unexperienced level. Far reaching changes to climate and everything within are already becoming evident (Ciais et al., 2013). The number of bushfires per year is increasing in Australia, partly because of warm, dry seasons caused by El-Nino climate oscillations (Bowman et al., 2009). It is estimated that bushfires contribute ~20% of global CO_2 emissions (Thonicke et al., 2010). These disturbance events cause changes in vegetation function and structure resulting in changes to landscape processes.

Calculating carbon stocks and fluxes has been of high international interest over the last two decades (Ciais et al., 2013). A key tension emerging from this effort is that processes influencing biosphere carbon capture vary greatly over space and through time, particularly those processes related to land surface characteristics (Beer et al., 2010). Landscape productivity is the GPP of all vegetative areas in a landscape, at regional to global scales. Methods to calculate this productivity have traditionally involved process-driven terrestrial biosphere models (TBMs) (Rogers et al., 2017). The emergence of accessible satellite technology has created a new data stream for climate and landscape researchers. This has allowed application of remote sensing (RS) to "extract new thematic information directly from remotely sensed imagery" (Jensen, 2007). A data-driven approach to modelling, with consistent geographical and temporal representation is developing, simplifying TBMs in the process. These models are ideally suited to disturbance events which have dispersed spatial impacts over long periods (Turner et al., 2006a). This analysis can be fed back to large scale models to further refine assumptions.

Many systems determine GPP, including vegetation traits. One universal trait is the presence of chlorophyll in the flesh of productive individuals, which reflect green light when exposed to solar radiation. RS of GPP seeks to capture the dynamics in plant chlorophyll content (Tucker and Sellers, 1986). Diagnostic models built on the basis of these spectral signatures are increasingly accurate (Zhang et al., 2017). They have been applied at large scales in the interest of carbon fluxes (e.g. Zhao et al., 2005; Jung *et al.*, 2009). However, downscaling these is considered important for analysing regional fluctuations in ecosystem processes (e.g. Goulden *et al.*, 2011). With frequency of disturbance changing in a rapidly changing climate (Bradstock, 2010), studying model response to these disturbances is critical, particularly if applied across disturbance boundaries.

The first chapters will introduce how GPP is measured across scales using RS and the biophysical underpinnings elaborated. Theory of fire severity and landscape processes in the

context of vegetation regrowth will follow. Later, a methodology based on a published global productivity model and fire severity is introduced.

1.1 Context

Bushfire is a major disturbance of vegetation and productivity worldwide. It impacts vegetation dynamically, disturbing carbon stocks and fluxes of vegetation. Burning biomass is estimated to contribute ~20% of global CO_2 emissions (Thonicke et al., 2010) and ~50% of NO_x and CO emissions annually (Ii and Carmichael, 2002). While direct emissions are the dominant carbon balance impact from fire in vegetation, there is also a lost potential productivity while landscapes recover from fire. This response is determined by many factors relating to canopy ecophysiology, including regeneration strategies and characteristics of the fire itself. The fire intensity is dependent on the fuel biomass and availability (to ignite), as well as fire weather conditions, which are all related to the regime of that landscape in terms of feedbacks between these characteristics and fire frequency (Bradstock, 2010). The fire impact is also dependent on the severity, which is the intensity as expressed through the affected vegetation (Keeley, 2009). In this way bushfire is intrinsically linked with vegetation productivity and landscape processes.

Here we refer to GPP (μmol C m^{-2} s^{-1}) as the product of photosynthesis at canopy scales in the context of landscape ecology. Landscape ecology is the functioning of the integrated biosphere and atmosphere and how these systems respond to ongoing disturbance. Photosynthesis is the primary process of landscapes with feedbacks to the atmosphere being a principal regulator of the global carbon cycle (Beer et al., 2010). Rates of productivity determine plant growth and levels of carbon sequestration. Understanding the drivers of such fluxes is fundamental to landscape ecology, with large scale study necessary for this.

The characteristics of radiation reflected at landscape scales (e.g. 30m to 5km) is related to the composition and structure of the surface material, amongst other things. Remote sensing of radiation from satellites observes vegetation traits related to stomata and leaf activity from which rates of productivity can be inferred (Jensen, 2007). Canopy scale processes are estimated by light and plant interaction throughout the canopy (De Pury and Farquhar, 1997). Laboratory biology has informed the interpretation of leaf and biomass reflectance. Strong relationships exist between plant leaf traits and such spectral variables (Asrar et al., 1984). Canopy conductance is defined as the movement of H_20 or CO_2 through the leaf to atmosphere and vice versa. This aspect of physiology can be related to spectral features by considering the heat fluxes associated with this interaction (Monteith, 1972). These two factors, canopy conductance and irradiance, govern productivity estimates over large scales.

Chapter 2: Gross Primary Productivity modelling with remote sensing

Modelling of vegetation over a landscape can accurately determine gross primary production (GPP), from satellite images. The theory related to this method is expansive and requires understanding of multiscale process from the leaves of vegetation to atmospheric interference in images of the landscape. The following discussion will focus only on those aspects of plant physiology that directly relate to remotely sensed (RS) GPP canopy models and their parameters, as distinct from the biophysics at the leaf or sub-leaf scale. Satellite sampling of ecosystems enables spatial and temporal investigation, unavailable in plot based work. This flexibility allows analysis of structural attributes and parameterisation of models of ecosystem processes. Resource use efficiency models look from the top down, considering how the productivity of a system in spectral space relates to the output of complex processes in situ. Many approaches have been developed for calculating GPP, with a range of resource use limiting factors included. The study of GPP after fire using these models highlights the ability of these factors to describe disturbed ecosystems.

2.1 Capabilities of satellite sampling

Satellite sampling or imaging of landscapes has enabled the characterisation of complex ecological processes with timeliness and spatial discretion. RS sensors capture solar energy reflected from the surface, or near surface, of earth. The relative reflectance of particular electromagnetic wavelengths by a material is related to the quality of that material (Jensen, 2007). RS is enabled by extensive satellite imaging and reference to a continental network of ground sampling sites. The FLUXNET system of towers measure fine scale meteorology and fluxes of carbon and water, using eddy covariance methods, between the atmosphere and terrestrial biosphere (Jung, 2009). This sampling style is mimicked in RS where an exchange of light energy is the characteristic of interest between biosphere and atmosphere, and the distribution of sample sites is almost universal (Schaaf and Wang, 2015). Conceptually RS and FLUXNET sampling are parallel, considering both measure landscape scale vegetation fluxes. The RS approach is popular due to the deployment of fine temporal and spatial resolution satellite sensors (Drusch et al., 2012) and increased interest in climate change. In global change ecology vegetation is a dynamic agent through which transfers of energy are large (Beer et al., 2010). RS is the measurement of these fluxes and the derivation of biophysical processes, such as productivity with newfound consistency.

2.2 Differentiating between modelling concepts

RS models of GPP at canopy scales require less data collection and parameterisation than more complex physiological models. RS GPP diagnostic models can be conceptualised as top-

down, data-driven approaches (Roxburgh et al., 2004). This approach represents just the necessary physiological processes to produce good model performance, in terms of final output (Yebra et al., 2013b). Physiological models of GPP aim to represent the ecosystem from the bottom up, including parameters from many sub-systems which interact with photosynthetic productivity (Rogers et al., 2017). For instance, the JULES model requires soil moisture, critical soil moisture concentrations for vegetation types and nitrogen distribution through the canopy as ecosystem specific parameters, amongst others (Clark et al., 2011). This complex parameterisation is a burden when multiple canopies or landscapes are of interest. The RS approach looks directly to the emergent properties of the physiology at large scales, rather than building a complex system to recreate such phenomenon (Fisher et al., 2015). Incorporating satellite sampling with top-down design, creates a pragmatic GPP modelling approach which has recently proliferated in earth system modelling.

2.3 The resource use basis

Top-down diagnostic GPP models simplify earth system model parameterisation, often by presenting the function of a plant or group of plants, as the capacity to use a finite resource. Monteith (1972) developed a light use efficiency formula for agricultural vegetation. It was derived from mesic and nutrient-rich conditions, although it has been shown to apply in most environments (Hilker et al., 2011). This is possibly due to the strong linearity between assimilation by photosynthesis and the absorbed incident solar radiation by leaves (**Equation 1**).

$$A = \varepsilon \times \mathrm{fPAR} \times \mathrm{PAR}$$

Equation 1 - Monteith's (1972) light use function.

Where A is GPP (μmol C m^{-2} s^{-1}), ε the efficiency of fixed carbon conversion, or LUE (mol C mol^{-1} photons), and fPAR the fraction of the absorbed photosynthetically available radiation (PAR, mol photons m^{-2} s^{-1}). This resource-use framework can include physical and biological constraints for situations where conditions are not optimal; including various solar interferences, environmental limitations on ε, as well as area (leaf or canopy) of productivity approximations. This mechanistic approach has great scope of application because radiation is necessary in all photosynthesis, and can be readily measured. This is true for remotely sensing and this radiation use framework has been adapted by a majority of models (Rogers et al., 2017).

2.4 Vegetation indices and model parameterisation

Vegetation indices are the predominant sampling approach to measuring primary productivity of vegetation remotely. The Normalised Difference Vegetation Index (NDVI) measures the ‘red-edge’ feature in the spectral response of a leaf target. Where high absorption in red wavelengths (0.62-0.67 μm) contrast strongly to low absorption in the NIR wavelengths (0.841-0.876 μm) (Rouse et al., 1973). This feature is characteristic of leaf chlorophyll pigment,

predominantly chlorophyll *b* (~0.64-0.67 µm) and associates the observed reflectance with carboxylation in the mesophyll. Chlorophyll molecules occur in the thylakoid membranes of chloroplasts and are necessary for the primary absorption of light photons penetrating the leaf structure (Collatz *et al.*, 1991). Converted energy is then transferred to the photosynthesis process. Abundance of chlorophyll is therefore indicative of high photosynthetic capacity (Sims and Gamon, 2002). As a representation of this pigment, NDVI provides an indicator of productive potential through the proxy of radiation pathways to carboxylase reduction (Goerner et al., 2011). The normalised difference is taken between groups of NIR and red wavelengths, most commonly Moderate Resolution Imaging Spectroradiometer (MODIS) reflectance bands ρ2 and ρ1 respectively; producing a relative scale of 'green area' or foliage cover (Tucker, 1979; Justice et al., 1998). NDVI provides a simple, indirect measurement of vegetation structural status, relates well to process parameters and can be sampled by satellite.

Calculating primary productivity of a canopy requires an estimate of the area of that canopy that is photosynthetically active. LAI is defined as the green leaf area per unit of ground area when considering one side of the leaf (Nemani and Running, 1989). NDVI is also linearly related to Leaf Area Index (LAI) when LAI < ~0.3 (Tucker, 1979). Though NDVI is representative of leaf area, it is not representative of how leaves necessarily interact with sunlight (Fensholt, Sandholt and Rasmussen, 2004). Photosynthetically available radiation (PAR) is the section of incident radiation (Q) that provides energy for primary productivity (~0.4-0.7 µm). A schematic of radiation interacting with plant leaves can be seen below (Figure 2), highlighting the interaction of radiation (PAR) with the 'green' chloroplasts in leaf cells.

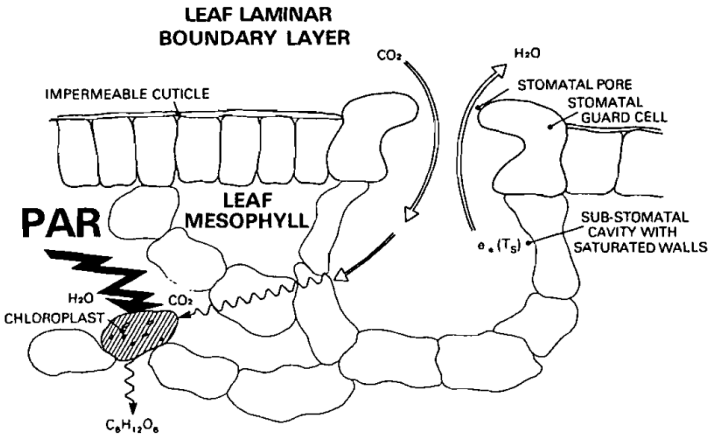

Figure 1 Radiation, water vapour and CO2 flux of leaves (Tucker and Sellers, 1986)**.**

If the relative area of photosynthetically active targets (i.e. NDVI) is known the fraction of intercepted PAR (fPAR) can be calculated based on empirical scaling. When this is combined with PAR (**Equation 1**), the total energy available to the canopy for photosynthesis can be estimated (Asrar et al., 1984). fPAR is scalable across species and plant functional types (PFT) (Gamon et

al., 1995). Ecosystem process models often use this as a starting parameter to estimate exchange between biosphere and atmosphere (Monteith, 1972).

GPP models of disturbance events require regular temporal sampling, to accurately capture change due to discrete events. The MODIS sensor, deployed on satellites Terra (1999) and Aqua (2002) passively measure radiation emitted or reflected by earth's surface in the visible to thermal infrared (0.6 to 14 μm) range (Justice et al., 1998). The sensors move in opposed orbit, creating daily coverage of global, spectral reflectance images, with a finest scale of 250m. Seasonal changes in canopies and landscapes are well sampled. Intra-seasonal changes, such as short term changes in canopy processes due to fire, are also well captured at this resolution (Gharun et al., 2018). Contemporary sensors have finer spatial and radiometric resolutions (Coyle et al., 2015). However, the temporal resolution and established theory of MODIS enable research on primary production. The Enhanced Vegetation Index (EVI) is another remotely sensed vegetation index that is used for exploring radiation pathways into primary production. It was developed partly in response to the problem of NDVI saturation in dense biomass such as tropical wet forest. This problem is function of the canopy background interfering with the canopy response within the pixel, resulting in overestimation (Huete et al., 2002). EVI is similar to NDVI in sensing the red edge feature. However, EVI incorporates another spectral feature, making it more sensitive to complex canopies and correlating well with LAI and canopy architecture. Complimentary indices, EVI and NDVI, capture consistent spatial information about vegetation which can be related to GPP.

2.5 A range of model approaches

Explicitly including the water cycle in GPP models improves accuracy in xeric environments, where light resource use is never maximised (Yebra et al., 2015). Berry developed a GPP model on a novel formulation of LUE, incorporating an evapotranspiration component. Net radiation flux, based on surface albedo and temperature extremes, was combined with latent heat of evaporation and a multi leaf description of the canopy to produce total evapotranspiration. This was then divided into transpiration of leaves based on 3 leaf functional types and respective water fractions. GPP is calculated by combing an empirical estimate of WUE of photosynthesis with the transpired mass of water for all leaf types. The requirements of data on leaf functional types and associated water mass, and WUE are specific and substantial. Such biome specific studies often parameterise using a supervised classification of other spectral data. This is difficult without considerable field checking (Tempfli et al., 2001). GPP models that rely on field parameterisation detract from the utility of RS in post disturbance landscape analysis.

The light use efficiency GPP model has been shown to improve in accuracy when a diffuse fraction of solar radiation is included. The improvement is notable in wet, diffuse-light (cloudy) seasons (Yan et al., 2017). It has been shown that as the fraction of diffuse radiation increases

(that is the portion passing through the upper layer of canopy) so too does assimilation of the whole canopy (De Pury and Farquhar, 1997). This is indicative of the presence of complex canopy structure where assimilating leaves and plants occur through the vertical profile, not just on the upper surface. Also leaves occurring at angles other than horizontal potentially absorb greater irradiance, as diffuse radiation has no uniform directionality (Mercado et al., 2009). Donohue (2014) confirmed the formulation of Roderick *et al.* (2001) by adding a diffuse component to a light use model parameterised with RS NDVI, which performed well across Australia. However the calculation of the fraction in the original work was shown to respond unpredictably when atmospheric particulates, namely a volcanic eruption, were present (Roderick et al., 2001). It is problematic to include this model component when considering large fire events, as the smoke may increase the diffusivity of incoming solar radiation in a diffuse fertilisation effect (Park et al., 2018). However interference with satellite samples may be short as smoke clears quickly. Given this uncertainty, GPP after fire is not considered relevant to diffuse radiation delivery.

Studies calculating GPP from satellite data most often use the light use efficiency framework. It was popularised by the authors of the MODIS global GPP product (MOD17, Running *et al.*, 2004). They take the light use efficiency of vegetation based on an empirical maximum for broad classes of biomes, combining this with a measure of the fraction of radiation available for plant photosynthesis (fPAR, where NDVI is proxy), and solar radiation levels. A further two environmental limitations, temperature and vapour pressure deficit, are applied as restraints on the maximum LUE variable representing varying physiological light use efficiency. A major problem with this approach is the lack of explicit moisture representation. A deficit of soil moisture tends reduce stomatal conductance and eventually GPP and evapotranspiration. This is the case in many dryland areas of Australia (Andela et al., 2013). In the MOD17 framework, environmental scalars do not represents this, nor the resultant decrease in productivity that may only emerge through NDVI latterly. In dry and semi-arid, Australian, fire prone, ecosystems this inability to respond to soil moisture is inadequate when modelling GPP.

The CASA model of Potter *et al.* (1993) incorporates soil moisture into a GPP, light use framework that can be adapted to RS (Field, Randerson and Malmström, 1995). The light use efficiency term is reduced by a factor equivalent to the difference in pan and potential evaporation. Assuming that the remaining potential is stored as soil moisture. In effect LUE is allowed to vary within seasonal limits relating to available moisture to vegetation. A maximum moisture constraint is used, for the case of fPAR also exhibiting effects of long term deficiencies. Where the reduction in leaf area due to lack of water translates to lower RS NDVI hence fPAR. This component may be parameterised by remote sensing making it accessible to cross biome studies. However the assumption that surplus potential evaporation becomes available to the vegetation is considerable. The inclusion of this restrain on LUE recognises the limit of water in GPP estimation. Models that consider canopy conductance separately to LUE achieve the same goal.

Including canopy conductance to carbon in modelled GPP can overcome some of issues of radiation alone. These include the expense of field checking and the separation of water use efficiency from GPP. Evapotranspiration can be derived from the inversion of the conductance term of the Penman-Monteith equation (Monteith, 1965; Monteith and Unsworth, 2013), (Equation 1). The P-M formulation considers the rate of evaporation of the canopy to be in proportion to the flux of heat. At the leaf boundary stomata are gatekeepers for this heat flux, comprised of water vapour and atmospheric CO2 exchange. Stomatal resistance is a primary control of the rate of carbon assimilation to sites of photosynthesis in the mesophyll cells (Leuning et al., 1995). This resistance is decided by many biotic and abiotic factors however it is always characterised by relative pressure of CO2 and water vapour molecules (Cowan and Farquhar, 1977). This recognition is uncommon in most radiation driven GPP models (e.g. Running, Glassy and Thornton, 1999). Mechanisms controlling stomatal activity are many whereas those on radiation productivity are theoretically simplified. Many fire prone landscapes have dry and hot climates, at least seasonally, creating requisite fuel (Chuvieco, 2009). Also, persistent low humidity and soil moisture are common during the warm season (Lauer and Boyer, 1992). Here GPP may be limited by conductance, due to the non-linear response to radiation at extreme (both low and high) conditions (Wu et al., 2015). Introducing conductance limitation into models reduces errors in GPP estimation, in arid conditions, where over estimation is likely (Yebra *et al*., 2015: Fig 3). Considering the action of stomata of leaves in fire prone ecosystems improves modelling of GPP.

Chapter 3: Fire disturbance and vegetation regrowth

RS GPP modelling has future potential capacity for monitoring ecological impacts of fire. While RS is utilised successfully for predictive purposes, such as fuel monitoring (Yebra *et al.*, 2013), fire detection (Giglio *et al*., 2016) and infrastructure protection (Chuvieco, 2009), there is scope for tracking the recovery of ecosystems. Plot based measurements are utilised to infer recovery condition for various structural metrics in regrowing vegetation. For instance, basal area, canopy cover, and tree height may be measured through time or across a chronosequence of samples representing different growth ages (Ruiz, Fandiño and Chazdon, 2005). However repetition of these samples is difficult and the construction of time-since fire series' thereby limited (Bartels et al., 2016). Also, in the absence of direct measures of ecosystem processes, like GPP, trends between field sample points are less certainly estimated, due to high variability within and between ecosystems (Beer et al., 2010). This variability depends on severity of fire, systems of regeneration and the accuracy of remotely monitoring these. Considering these, integration of GPP and fire analysis with RS modelling is highly useful.

3.1 Fire severity and regeneration

GPP rates of burnt vegetation are influenced by the impacts caused by fire characteristics. Severity is a measure of the effects on vegetation, related indirectly to intensity, during combustion (Keeley, 2009). It is considered an ecosystem attribute and not a fire characteristic. Severity indicates the inability for fire to disturb combustible material given that response may vary among and within vegetation groups given the same measurable fire intensity. High severity is broadly classified as near complete combustion of over storey, while low severity is a ground fire with no prescription of combustion.

Fire effects are relative to landscape characteristics. This complicates recovery analysis, where structural attributes, such as regeneration strategies vary. The differenced normalised burn ratio (dNBR) is a commonly applied VI, observing the negative change of reflectance in the near infrared (NIR) and positive in the short-wave infra-red (SWIR) after fire (Lutes et al., 2006). The former is associated with the loss of chlorophyll containing targets, in the spectral signature, that occurs with leaf scorching, like the NDVI. Whereas, SWIR occurs with higher presence of woody targets, often as standing dead wood or exposed bark post fire. Two images, before and after, are differenced to see the absolute changes in that vegetation. This assumes that the samples are seasonally aligned with a similar soil moisture content (Lutes et al., 2006). Differencing between these values is prone to error, particularly in heterogeneous ecosystems or when comparing effects between bushfires (Kokaly et al., 2007). If a vegetated site displays lower spectral reflectance in both observed frequencies because of a sparse canopy structure, comparison to a more vegetated site renders the absolute difference of NBR less when experiencing the same fire

intensity. Therefore comparing absolute differences in severity measure is considered less useful across sites (Edwards et al., 2013). In this case a relativised dNBR is a useful adaption which includes pre-fire vegetation condition in the change detection (Parks *et al.,* 2014) Severity can be measured spectrally as vegetation responds to fire intensity and is related to ecosystem processes.

Tree mortality and regenerative approach of vegetation are factors in GPP recovery of fire prone ecosystems (Odum, 2014). Obligate re-sprouting species grow lignotubers in the roots, or epicormic buds under the bark. These features allow vegetative regrowth of individuals following disturbance (Nicolle, 2006). These communities comprise much of the mixed Eucalyptus forests of south-east Australia. The obligate reseeding technique relies on canopy seed and is most successful in a fire regime of extreme events with complete canopy scorch (Vivian et al., 2008). Montane wet forests contain such species (e.g. Mountain Ash, *Eucalyptus regnans*) (Nicolle, 2006). Recent research in other mixed forests of pre-dominantly re-sprouters has shown that reseeding approaches may also be utilised here, after severe fires. Mortality was very high, reducing re-sprouting capacity, with significant seedling recruitment occurred compared to areas of moderate to low severity (Bennett *et al*., 2016). These facultative re-seeders are exemplified by Brown Barrell (*Eucalyptus fastigata)* of mountainous ACT. Fire adapted, re-sprouting communities, which are dominant in SE Australia, may experience structural change in extreme events, potentially affecting ecosystem processes. Such species trait are factors in GPP following fire of different severity.

In canopies that experience no or low scorch, regeneration may be suppressed and GPP less affected. The survival of over storey individuals in obligate seeding forests increases competition in the lower stratum following fire, predominantly by reduced available light and moisture to seedlings (Bennett et al., 2016). The survival of these new individuals is low and there is little impact on the structure of the dominant individuals where canopy cover is maintained (Vivian et al., 2008). In these tall and closed forests, indices, particularly the NDVI, saturate at high values due to complex canopy structure (Huete et al., 2002). Any regeneration in the understorey is disguised by survival of the pre-fire canopy, potentially leading to underestimates of the photosynthetically active area for post-fire years. However, the high mortality of seedling regrowth, due to competition with canopy, constrains major effects on ecosystem structure and RS response. In mixed forest, again the canopy remains intact and seedlings may shoot in the understorey of facultative species, however there is epicormic and lignotuber regrowth in all stratums. This growth is not suppressed, and may flourish in the niches created by patchy mortality of over storey. Seedlings on the ground storey are likely killed by further low severity fire, particularly in fire managed areas (Bennett *et al*., 2016). The interplay between regrowth strategy and canopy survival is important for RS modelling of GPP capacity.

Remote sensing of low-severity fire in grasslands has shown a reduction in primary production, using EVI as proxy, when validated with flux towers (Rocha and Shaver, 2011). Such analysis is successful in ecosystems with simple canopy structure. However, in closed forests, the

rdNBR index has proven less accurate in identifying low-impact areas (25% user accuracy) compared to high-impact (56.3) or no impact (92%). This study was validated with field samples in the Victorian montane forests (Bennett *et al*., 2016). It shows the difficulty of sensing restricted regrowth, particularly of re-sprouting or facultative forests, within complex stand structure. GPP models built on RS indices may suffer decreased accuracy for relatively low regeneration events, however severe fires and subsequent regrowth provide spectral definition for assessment.

3.2 Vegetation regrowth and changing productivity

GPP associated with regrowth is affected by structural changes, and physiological changes in the canopy. Burning reduces leaf area causing a loss of ability to intercept radiation and productive potential (Ehleringer and Field, 1993). This can be as severe as near-complete GPP loss associated with death of over storey in fire-sensitive, temperate, montane forests (Buckley et al., 2012). Contrastingly, a reduction of 30% GPP has been estimated in tropical forests after uncommon high severity events (Biswas, Lasko and Vadrevu, 2015). As new leaves expand, through different regeneration strategies the canopy area returns and the capacity for productivity increases (Fleck et al., 1998). This expansion is critical for modelling GPP after fire using satellites.

With a restored capacity for GPP the actual rate of productivity per leaf varies through time, regardless of environmental limitations placed on LUE (Russel, Marshall and Jarvis, 1989). The leaf GPP is often referred to as the photochemical efficiency. This rate depends on the maturation of leaf scale photosynthetic components. For instance photosynthetic pigment to protein ratios change with age for many species (Šesták and Šiffel, 1997). This variation in photochemical efficiency means fraction of absorbed photosynthetically available radiation (fAPAR) is often overestimated, particularly after disturbance events (Cheng et al., 2006). The authors showed NDVI based fAPAR to remain highly positive, with complete canopy loss, while field measurements dropped near zero. In the case of steady fAPAR, or productive area, a time averaged LUE term, will reflect the efficiency of the productive area. This assumes that under optimal meteorological conditions, canopies reach their maximum physiological potential. However the limit of photochemical efficiency through time may still be present, more so in young vegetation. Zhou *et al.* (2015) found maximum LUE to increase for the first 17 years of growth in evergreen needle leaf forests. This finding suggests, holding LUE fixed through time will underestimate GPP of younger canopies, leading to inaccuracies in vegetation recovering from fire and overestimation in old growth. If diagnostic GPP models are to be applied to carbon accounting, considering large scale disturbance, this uncertainty needs to be addressed.

Combining time and ecosystem dependence of LUE improves GPP modelling. However this parameterisation is complex, due to the high spatial variability of both characteristics during stochastic disturbance. Madani *et al.* (2014) used classification of forest stand age across Canada

(Pan et al., 2011) to determine canopy traits such as nitrogen content and effects on GPP using a LUE term. They also suggested further investigation into LUE in terms of leaf trait variations through time. This is beyond the scope of this research, however some of this uncertainty may be compensated for by employing the conductance component which does not rely on fPAR based LUE. Also Buckley *et al.* (2012) found, in Mountian Ash forests of Victoria, that photosynthetic potential measured in the field did not vary between seven-year regeneration, after stand replacement, and old growth forest (71 yrs). Suggesting that productive potential of the leaf and the canopy are quickly recovered in these forests. This is for high severity fire, where canopy is removed. If the adjustment of photochemical efficiency is relative to the expansion of fPAR in regrowing vegetation, GPP estimates using unrestrained LUE may be effective. In many ecosystems including conifer forests of Oregan USA this is not the case (Turner et al., 2006b). Stand age affects GPP across a range of burnt and logged forests. Here a scalar is applied to the LUE term (ε, **Equation 1**) of GPP, based on a vegetation age layer. This input is from extensive and intensive field data collation. For large heterogeneous landscapes, without prior research, this is more difficult. RS GPP models assessing disturbance require further parameterisation of LUE through time.

Furthermore fire can induce structural change due to vegetation succession (Huang et al., 2013). Given an event where the regeneration strategy of the dominant vegetation destroyed is insufficient to compete, an overall shift in vegetation extent may occur. The succeeding species may be a historically lower storey species that suppresses over storey regeneration leading to dominance of a different ecosystem structure. To overcome these dynamics when estimating GPP after fire, parameters must be drawn from multi-species attributes. Where the structural difference of the open-forest compared to the closed-shrub land, for instance, is perceptible in spectral space. Also, a vegetation classification of spectral space may preclude a temporal shift in relative extent. The vegetation index approach of GPP modelling accounts for structural variation due to the correlation of such indices with leaf area index (e.g. Yebra *et al* 2015 in section 2.2). In turn this characteristic relates to vegetation height and other elements of structure. Different indices may be applied as representation of productive area, or combined in average representation of structurally dissimilar biomes.

Water use efficiency (WUE) is an important factor in GPP of regrowth. WUE is the ratio of units of CO_2 assimilated to units of H_2O lost (Donohue, Roderick and McVicar, 2007). The lower LAI of regrowth vegetation reduces evapotranspiration due to lack of interception. Often increasing soil moisture availability in the short term (Fleck et al., 1998). Conversely young vegetation, regrowing from seed has higher WUE as the plant attempts to assimilate more carbon for plant growth (Flexas, Loreto and Medrano, 2011). The competition between CO_2 substrate and transpiring moisture through the leaf space defines this trade-off, as both fluxes are necessary for plant growth (Hetherington, Smillie and Davies, 1998). Most species have adapted to this compromise by rapidly (minutes - hours) adjusting stomatal conductance. During regrowth after

fire the expanding canopy increases ET as well as adjusting stomata to balance high assimilation with increasing transpiration (Choinski, Ralph and Eamus, 2003). Resulting in lowered soil moisture and training of work toward maintenance of fixed plant material (Cernusak et al., 2006). ET has shown to increase significantly in seedling regrowth forest where a majority of individual mortality occurred, compared to pre-fire levels (Brookhouse, Farquhar and Roderick, 2013). This resulted in an observable streamflow reduction in effected catchments. However in mixed eucalypt forests in less fertile landscapes this large increase in ET was less and extended over a 15 year period post fire (Nolan et al., 2015). GPP models that describe the relation between ET and GPP are more suited to post-fire environments.

Chapter 4: Aims and hypothesis

This research is aimed at studying GPP across Australian vegetation types and the different impacts fire has on carbon flux. Of interest is the influence of fire severity and vegetation type. Analysing these components will highlight ongoing changes to landscape productivity due to disturbance. To do this a recently developed model by Yebra *et al.* (2015) is downscaled and analysed on new study sites. The original paper estimated GPP across 16 sites and globally, considering radiation and canopy conductance as drivers. This paper does the same at finer resolution across bushfire events, within the MODIS satellite data record. This application will calculate long term trends in GPP recovery of landscapes, considering that severity is likely a driver of vegetation response. Differentiating between low and high severity areas and classes of vegetation affected, determines the response of post-fire GPP relative to unburnt control locations. It is expected that fire severity is the dominant driver of GPP recovery. The hypotheses are:

- GPP recovery time is dependent on burn severity.
- GPP recovery time is dependent on vegetation type.

In order to verify the hypothesis the following questions are considered:

- How do rates of productivity trend with time after fire?
- How does this rate differ by severity within the fire scar?
- How does this rate differ by vegetation type?
- Do remotely sensed models sufficiently capture this variation?
- What does the variation in productivity suggest of the vegetation types?
- What does the variation in productivity suggest of the RS approach to fire response?

Chapter 5: Methodology

5.1 Overall Approach

Vegetation was sampled from four study sites that were affected by large fires, using an index of burn severity (see 5.4.3, p.25). Each group of samples was paired with control areas outside the firescar. A satellite based GPP model was then run for the region of each study fire, based on 4 day satellite return, including the calender year prior. The groups of samples were averaged across the landscapes and timeseries produced for each.

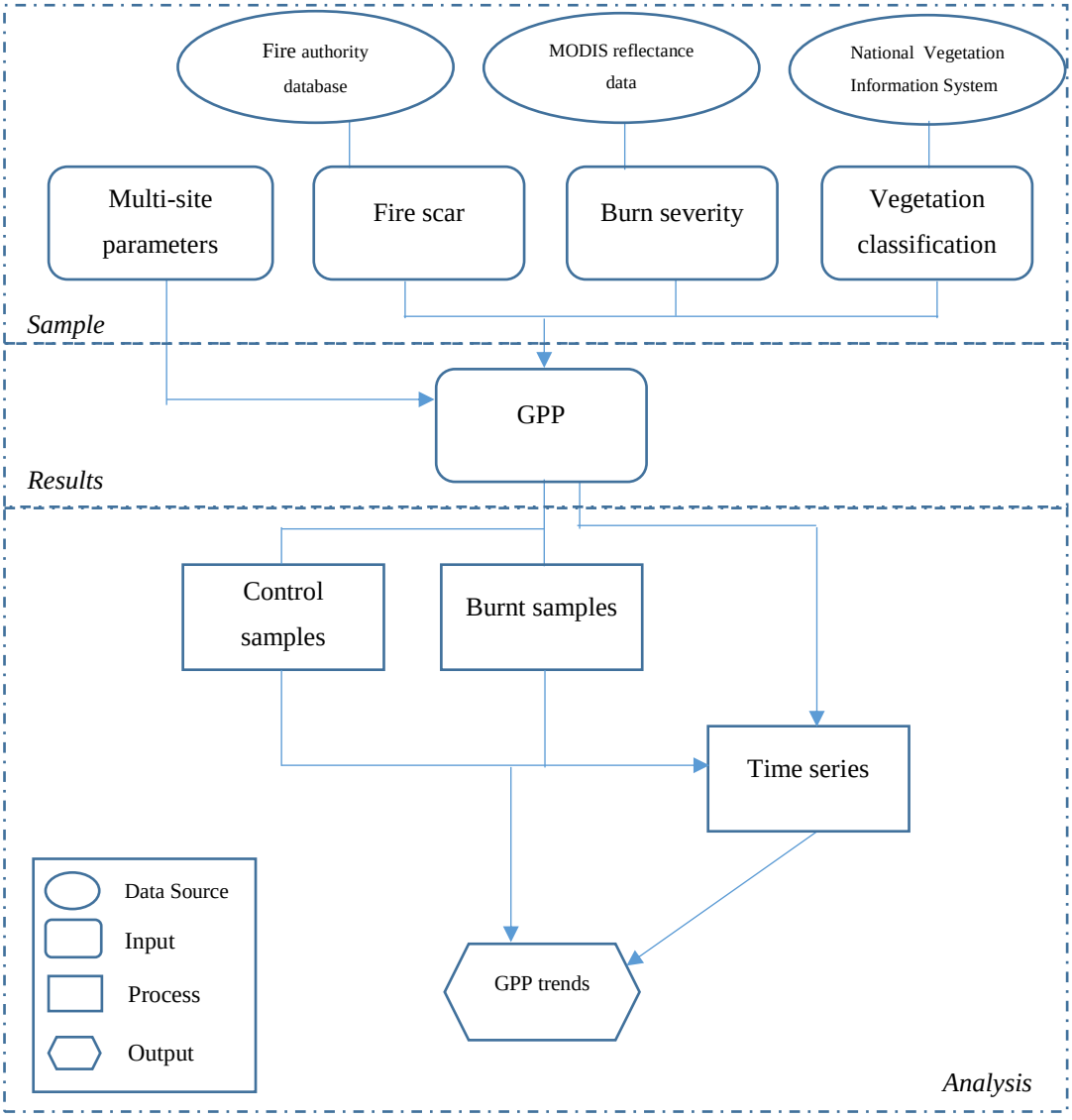

Figure 2 Methods conceptual diagram

5.2 Model description

The remotely sensed GPP model of Yebra *et al.* (2015) is shown, diagrammatically in Figure 3. This approach uses the lesser of radiation or conductance limited GPP, parameterized with RS VIs. The components of conductance and radiation, Fc and Fr, respectively (μmol C m^{-2} s^{-1}), derived GPP both take a combination of MODIS reflectance data and meteorology as raw data inputs. Only two fitting parameters are required across biomes, one for each component. Fc is parametrized using an exponential equation (Equation 2) applied to vegetation indices, NDVI, EVI

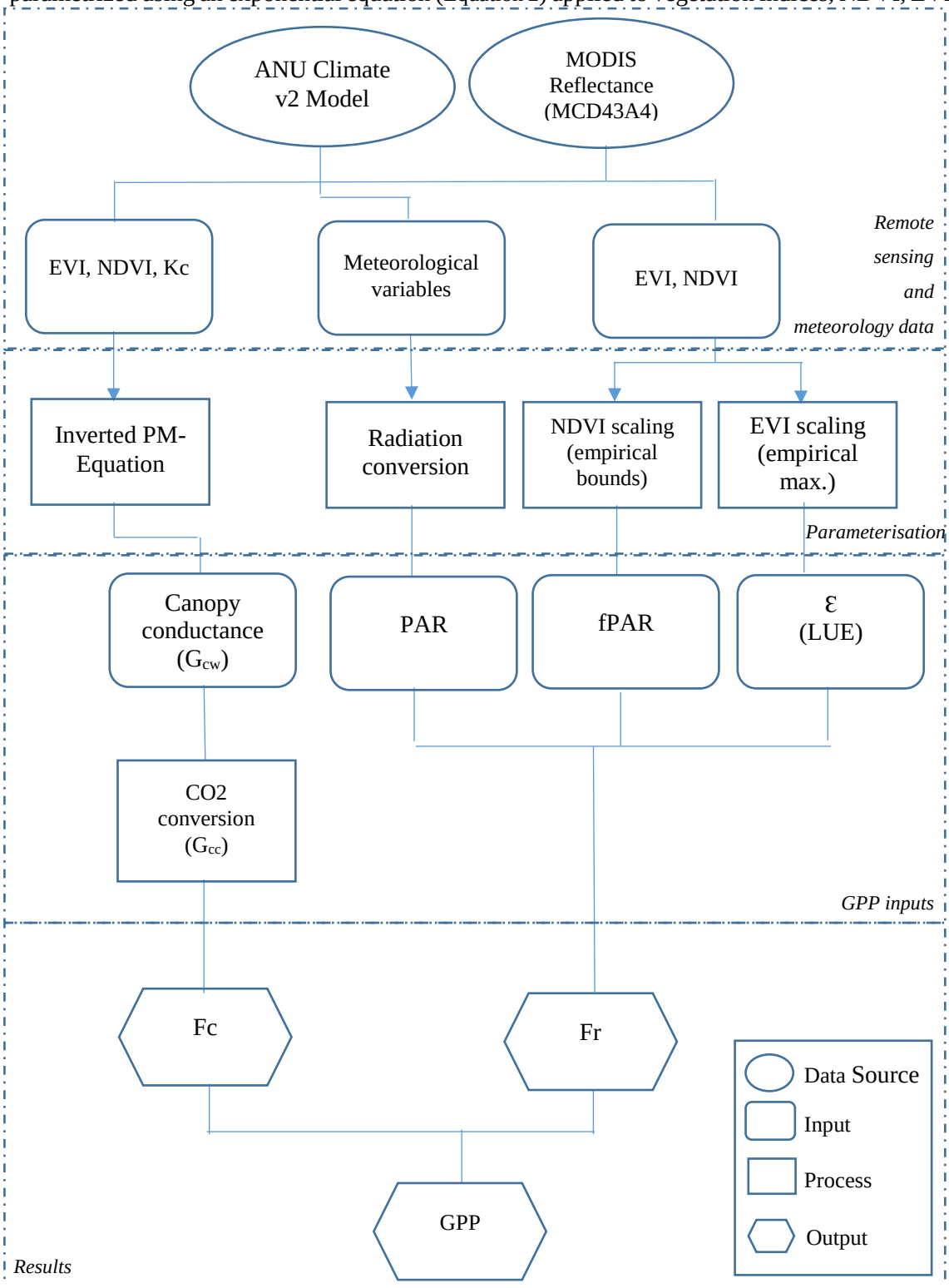

Figure 3 Yebra et al. (2015) method

and crop factor (Kc). This index combines the residual moisture index (RMI), rescaled EVI, and the global vegetation moisture index (GVMI), to describe the residual difference of moisture in the canopy through NIR reflectance. The canopy conductance to water vapor is produced by inversion of the Penman-Monteith formulation of latent heat flux and was validated by the authors at 16 FLUXNET sites in 6 different land cover types globally (Yebra *et al.*, 2013).

$$G_{cw} = a \exp[b\ (VI - VI_{min})$$

Equation 2 - Canopy conductance model developed by Yebra et al. (2013).

Where a and b are coefficients per VI and VI_{min} is the VI observed for bare soil, which Yebra *et al.* (2013) optimized after parameterizing values from literature, and the result, G_{cw}, is conductance to water vapour (mm s^{-1}). Best VI predictions varied between biomes (see 5.5). The average of the three computations of VIs was found to predict G_{cw} best overall ecosystems (Yebra *et al.*, 2013), which I then applied in a H_2O to CO_2 conductance conversion equation at each pixel (Equation 3).

$$F_c = c_g G_{cw}(1 - R_0)C_a$$

Equation 3 – GPP based on conductance to vapour at the leaf boundary.

Where F_c is the mean GPP (μmol C m^{-2} s^{-1}), c_g is the conversion coefficient of H_2O to CO_2 diffusion (mol C m^{-3}), G_{cw} is the canopy conductance to H_20 from the latent heat flux as described above (Equation 2), R_0 is the ratio of minimum achieved external (C_a) to internal (C_i) CO_2 pressure, and C_a is the atmospheric concentration of CO_2 derived from a quadratic equation based on samples at Mauna Loa, Hawaii (Equation 4). R_0 used here is based on the optimized value across all FLUXNET sites in Yebra *et al* (2015), and the same function used there to account for effect of vapor pressure deficit (VPD) was used here. R_0 is related to stomatal conductance and evapotranspiration, and varies by vegetation species and growing conditions (Kelliher et al., 1995). Values for woody species correlate reasonably well ($r^2 = 0.66$) with surface assimilation rates. However, the maximum ratio internal to external leaf CO_2 has been shown to occur throughout the day only if soil water availability is sufficiently high (mesic environment). Minimum ratios may be up to half (~0.3 compared to ~0.7) for soil that is significantly drier (Tuzet, Perrier and Leuning, 2003). This method assumes a limited range is maintained because this did not degrade model performance when tested at 16 Fluxnet sites (Yebra et al., 2015).

$$\boldsymbol{C_a = 1.206 \cdot 10^{-8} y^2 - 4.641 \cdot 10^{-5} y + 0.045}$$

Equation 4 – Atmospheric carbon concentration.

The Fr is taken from maximum light use efficiency by the canopy based on a scaled EVI, where the maximum value ε_{max} was optimised across the FLUXNET sites previously mentioned.

$$F_r = \varepsilon\ f_{PAR}\ Q$$

where $\varepsilon = \varepsilon_{max} EVI^*$ and

$$EVI^* = \max(\min\left(\frac{EVI-0.05}{0.90-0.05}, 1\right) 0)$$

Equation 5 - GPP based on radiation use efficiency of the canopy.

Where Fr (μmol C m^{-2} s^{-1}) is GPP, ε_{max} is the maximum light use efficiency optimised across biomes, represented spatially by scaled EVI, Q is incident radiation and f_{PAR} is that which is available to the canopy based on NDVI.

$$f_{PAR} = f_{PAR,max} NDVI^*$$

where $f_{PAR,max} = 0.95$ and

$$NDVI^* = \max\left(\min\left(\frac{NDVI-0.1}{0.9-0.1}, 1\right) 0\right).$$

Equation 6 - Fraction of interceptable radiation based on NDVI.

This formulation of radiation driven GPP uses Monteith's standard formulation of productive potential (Monteith, 1972) however the parameters are adapted for RS based on strong relationships between VIs and physiological attributes (Yebra et al., 2015; Zhao et al., 2005). It is noted that assuming leaf level GPP will be scaled accurately by indirect canopy area measurements may be vicarious; when fPAR is decoupled from actual productive area (Myneni, Los and Asrar, 1995).

F_r and F_c components were originally validated over the IGBP land cover classes; grassland, cropland, evergreen needle-leaf forest, evergreen broad-leaf forest and woody savanna (Yebra et al., 2015). These types include the variation within Australian study sites. Therefore parameters The output of GPP from the two components were then compared at each pixel so that the conservative estimate was produced (Equation 7).

$$\boldsymbol{F = \min(F_c, F_r)}$$

Equation 7 - GPP of lesser of two remotely sensed components.

5.3 Study Sites

The fires analysed here occurred in three temperate forest ecosystems, and one semi-arid shrub-land, Big-Desert Wilderness Park in south-eastern Australia (Figure 4 and Table 1). The Black-Saturday and Brindabella events were considered mega-fires, with widespread crown fires that covered areas of national park, reserves and private property. The four sites represent a range of fire characteristics, with Deua-NP having lower average intensity than the other forested sites.

Table 1 - Study site descriptions.

Location	Size (ha)	Date	Duration (days)	Vegetation	IGPB land cover classes	Reference
Brindabella and Namadgi NPs, Canberra, Australia	164,914	08/01/2003	14	Mixed Eucalyptus sp. and Alpine Ash forests, some Radiata pine	EBF, some ENF	(Mills, 2005)
Black Saturday fire, Victoria, Australia	400,000	07/02/2009	7	Mixed Eucalyptus sp. and Mountain Ash forests	EBF	(Hislop et al., 2018)
Big Desert Wilderness Park, Vic	181,400	17/12/2002	8	Shrub-land/Mallee shrub-land	OSH	(Esplin, Gill and Enright, 2003)
Deua National Park, NSW	46,000	24/12/2001	20	Mixed Eucalyptus sp.	EBF	No published literature

These fires (Table 1) are selected for their significant impact social impact and timeliness within the MODIS period. They have featured in some literature and represent a range of biomes (Table 1). The Black Saturday and Canberra 2003 have been researched elsewhere (e.g. Vivian *et al.*, 2008, Buckley *et al.*, 2012). Big-Desert Wilderness Park fire was the largest area burnt of any fire in the previous 20 years in Victoria (Esplin *et al.*, 2003). The Black-Saturday site is currently undergoing a shortening of the fire return period. This is due to the increased fire occurrence in obligate seeding forests, increasing high severity events in all forests types, and logging disturbance over the past century. Most of the Black-Saturday site burned in a large event in 1939 that extended along the Alps to meet the Brindabellas. Small sections of Brindabella fire scar have burned at various times before and since 2003, the largest being ~15% in the far southern section in September 1983. Deua fire scar burnt in the 1990/91 fire season, southerly, while the north eastern section burnt in bushfires in 1980/81. Periodical fuel management fires have occurred since 1991 (Yebra, 2018).

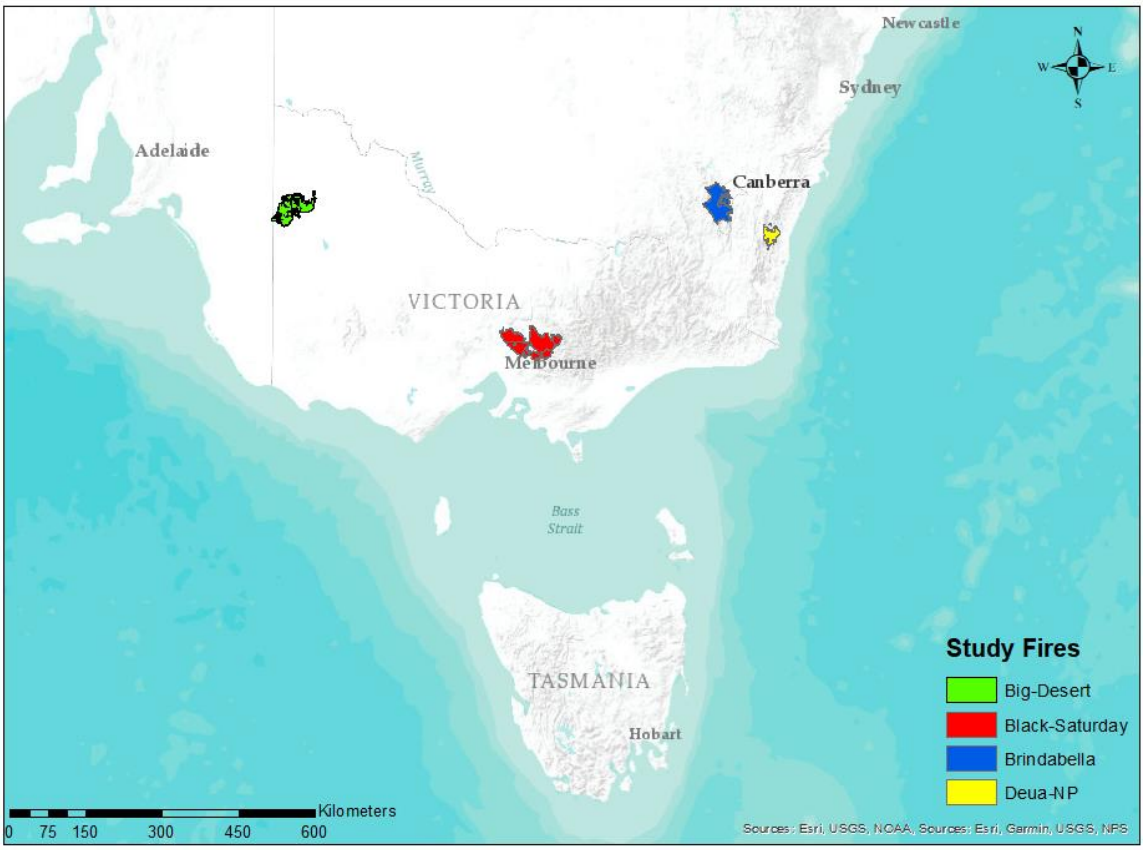

Figure 4 - Locations of study fires in South Eastern Australia.

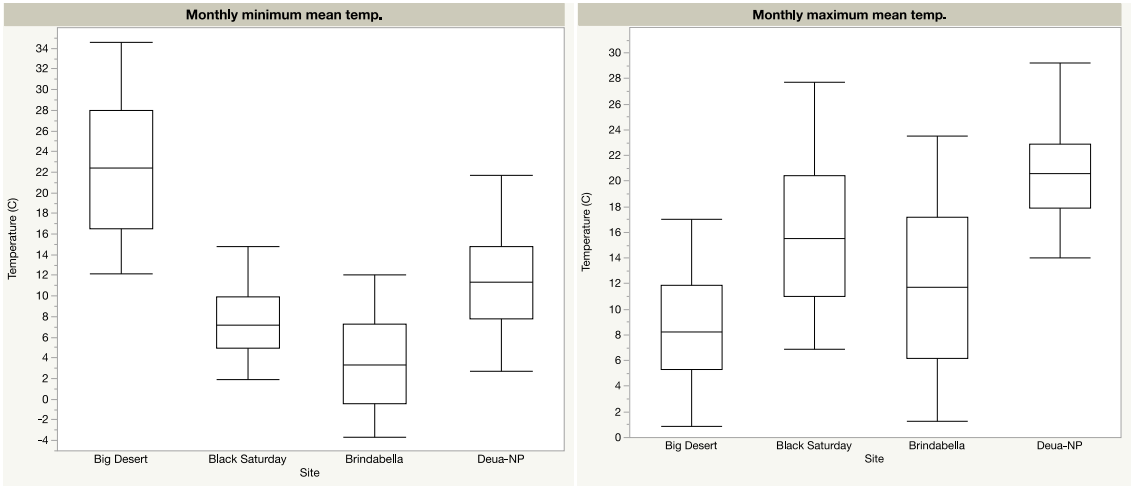

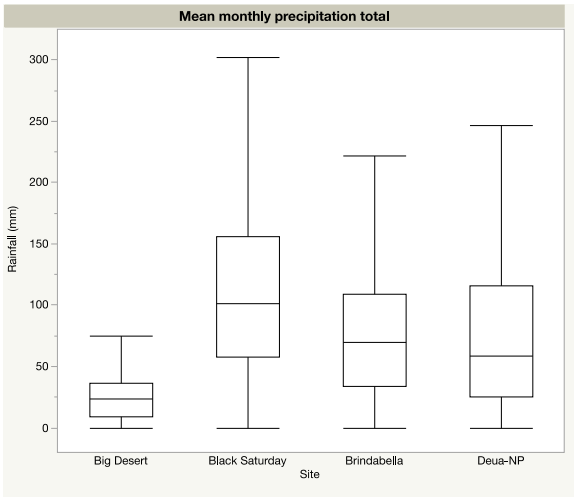

Figure 5 - Climatology of four sites in SE Australia.

5.3.1 Vegetation

The Brindabella site covers a range of open and less closed sclerophyllous vegetation communities across mountainous gradients with minor plantation forest (Table 2). Lower slopes comprise open forest with shrub understorey, down to grassy understorey at lowest elevations (Thomas, Gellie and Harrison, 2000). NDVI values are becoming saturated in the areas of *Eucalyptus* forest and in the apparent *P. radiata* plantations. EVI shows better discretion in the dense vegetation, (Figure 7). The city of Canberra can be seen to have random values, in the north east.

Table 2 - Species specific vegetation of study sites.

Brindabella	Position
Snow Gum (Eucalyptus. pauciflora)	Upper
Mountain Gum (E. dalrympleana)	Upper
Alpine Ash (E. delagatensis)	Upper
Brown Barrel (E. fastigata)	Upper
Apple Box (E. bridgesiana)	Upper/mid
Broad-leaved peppermint (E. dives)	Upper/mid
Brittle Gum (E. manifera)	Upper/mid
Candle bark Gum (E. rubida)	Lower
Radiata pine (P. radiata)	Lower
Black Saturday	
Mountain Ash (Eucalyptus regnans)	Upper
Alpine Ash (E. delagatensis)	Upper
Brown Stringybark (E. baxterii)	Mid/lower
Narrow-leaved Peppermint (E. radiata)	Mid/lower
Mountain Grey Gum (E. cypellocarpa)	Mid/lower
Messmate (E. obliqua)	Mid/lower
Eucalyptus low open woodlands with a shrubby understorey	Mid/lower
Other Acacia tall open shrublands and [tall] shrublands	Mid/lower
Big-Desert	
Slender-leaf Mallee (Eucalyptus leptophylla). Shrub species include, , and	Throughout
Yellow Mallee (E. incrassata)	
Scrub-pine (Callitris verrucosa)	
Dwarf She-oak (Casuarina pusilla)	
Desert Hakea (Hakea muelleriana)	
Green Teatree (Leptospermum coriaceum)	
Heath Tea-tree (L. myrsinoides)	
Desert Banksia (Banksia ornata).	
Porcupine Grass (Triodia irritans)	
Deua-NP	
White Ash (E. fraxinoides)	Throughout
Silvertop Ash (E. sieberi)	
Mountain Grey Gum (E. cypellocarpa)	

Messmate (E. obliqua)

Big-Desert Wilderness Park is predominantly a shrub-land of sparse coverage (~40% projected canopy cover) with a dispersed over storey of mallee. Over the sandy dunes and soils a ground layer of is common (National Parks Service and Department of Conservation and Natural Resources, 1994). NDVI values of the vegetation range from 0.21 - 0.39 (25th- 75th percentile), with a mean of 0.32 (Figure 6). The South Australian/Victoria border can we seen in the west.

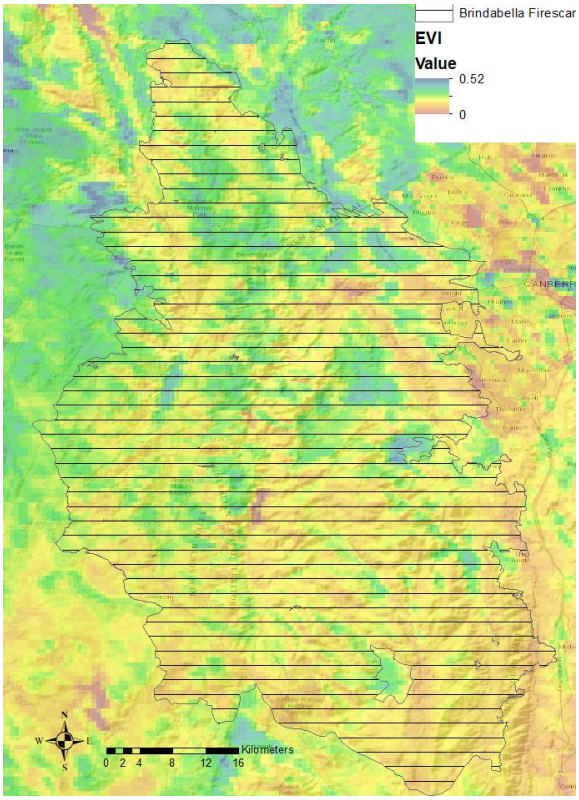

Figure 7 Image of Brindabella fire scar and mean EVI (2002-2016). Horizontal lines indicate area of fire scar.

The Black-Saturday fire occurred in 3 different catchments, north-east of Melbourne, Victoria. NDVI averages 0.67 with very high values (>~0.8) in the tall forests.

The Deua National Park site is predominantly is *Eucalyptus* woodlands containing a shrubby understory with ferns, sedges, rushes, and wet tussock

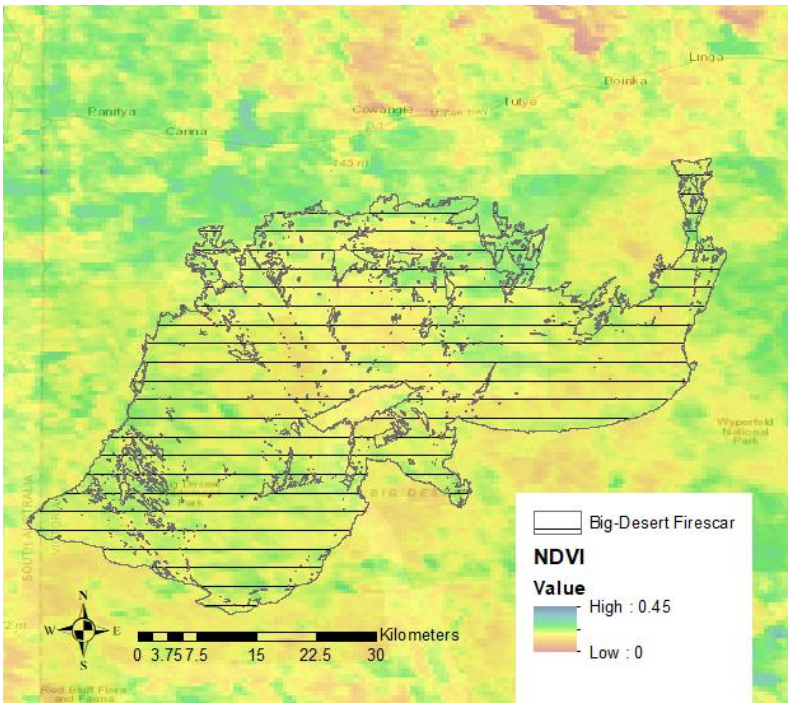

Figure 6 - Image of Big-Desert fire scar and mean NDVI (2002-2016). Horizontal lines indicate area of fire scar.

grasses in wetter locales persisting where tall open Eucalyptus forests dominate, with herbs

appearing concurrently (NVIS Technical Working Group, 2017). Species are similar to the middle to higher elevation Brindabella site. NDVI values range from 0.5 in drier gullies to >0.8 in tall forests.

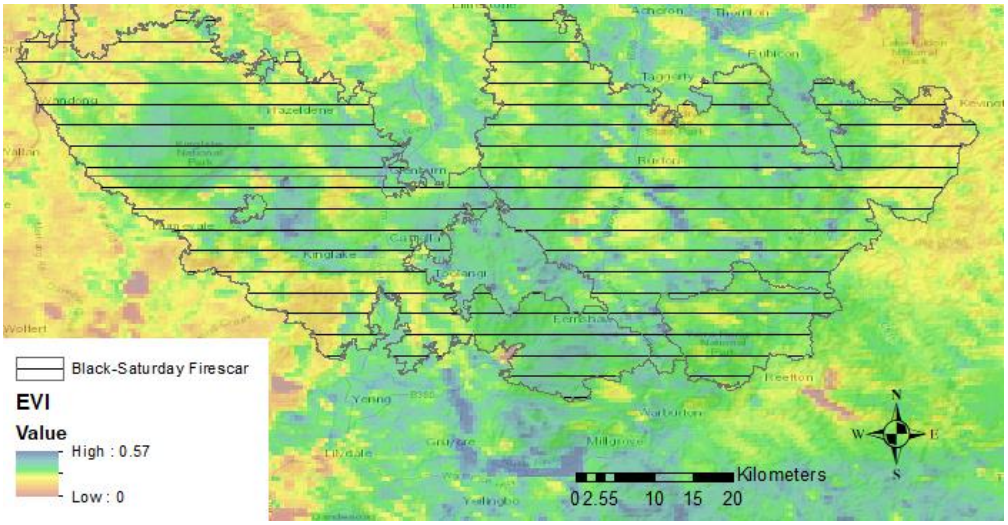

Figure 8 - Image of Black-Saturday fire scar and mean EVI (2008-2016) Horizontal lines indicate area of fire scar.

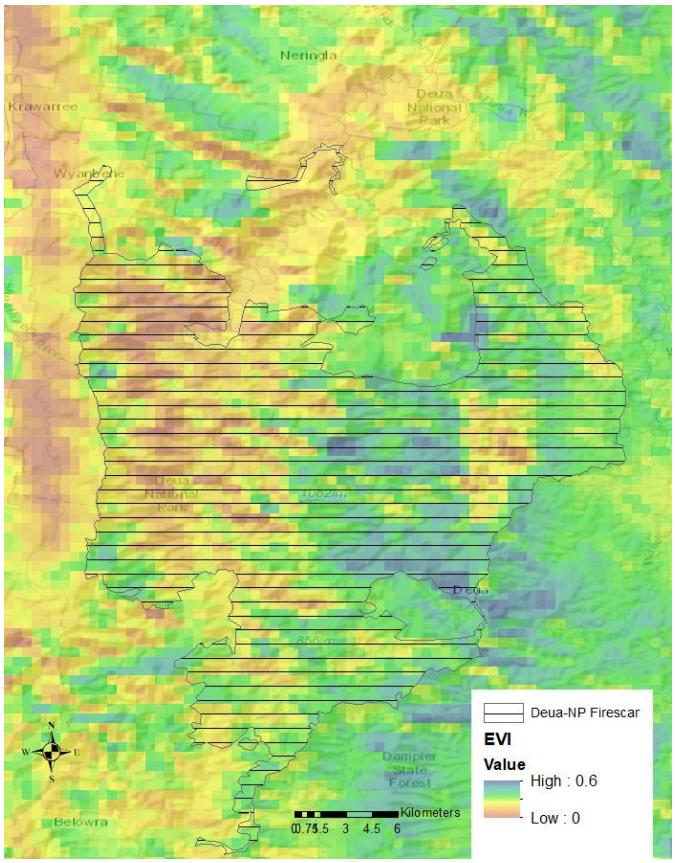

Figure 9 - Image of Deua-NP fire scar and mean EVI (2001-2016). Horizontal lines indicate area of fire scar.

5.4 Data

Satellite sources are open source; fire scar boundaries are from the relevant state authority, and meteorological inputs were taken from the recent version of ANU Climate model (Table 3).

Table 3 Spectral, meteorological and fire scar data sources

Data	Source		Resolution
Surface reflectance product	MODIS MCD43C4 Global Reflectance Product adjusted for Atmospheric and bi-directional errors (Schaaf and Wang, 2015)		0.005° grid
Continental meteorology (Daily surface radiation, maximum and minimum temperatures)	ANU Climate v2 Model (Hutchinson et al., 2018)		0.01° grid, resampled to 0.005° using cubic spline interpolation
Major vegetation subgroups	National Vegetation Information System (NVIS) (NVIS Technical Working Group, 2017)		100m raster, resampled to 0.005° using average resampling
Fire scar boundary	Site	Source (Yebra, 2018)	(Vector file)
	Brindabella	ACT Government	
	Black Saturday	Victorian Gov. Open Data Directory	
	Big-Desert	As above.	
	Deua-NP	NSW Office of Environment and Heritage	

5.4.1 Reflectance data

MODIS reflectance tiles, (MCD43A4, 500m resolution; Schaaf and Wang, 2015) produced by Land Processes Distributed Active Archive Center (LPDAAC), were acquired from the ANU Water and Landscapes Dynamics group via the National Computation Infrastructure (NCI) for each study area, over the longest time period possible. These images are adjusted with a bidirectional reflectance function to remove reflectance sun-target-sensor geometry issues. Images were then screened for poor quality using the built-in flags, with only the highest quality accepted. They were re-projected from sinusoidal to geographic coordinate system, WGS84 in the Numpy and Xarray python libraries, finally building a cube (latitude, longitude and time dimensions) of data for each site.

5.4.2 Meteorology

The ANU Climate Version 2.0 dataset is based on a range of station measurements from 1970 to the present. For the GPP radiation component, stable daily solar radiation was used. It is the total received in 24-hour period and is spatially interpolated based on temperature ranges and

rainfall. Temperatures (maximum and minimum) are the respective values averaged for the 24 hours after 9am, interpolated using exaggerated elevation and proximity to the coastline. VPD is the average of 9am and 3pm measurements at 300-700 stations, also interpolated using elevation and coastline.

5.4.3 Severity

Differenced normalised burn ratio (rdNBR) was used to measure vegetation response to fire impacts. The standard dNBR is an absolute measure of the fire caused change in NIR and SWIR signature of vegetation. To compare changes between sites, the pre-fire image of vegetation is used to create a relative change index. MODIS MC43A4 was again utilized for before and after images of the fire scar. Images were taken from the same season, to reduce effects of growth or senescence. The difference between images highlights response of vegetation to structure change (Key and Benson, 2006) across the fire period considering that pre-fire values are inherently different between sites (Equation 8). The index predominantly represents a reduction in moisture and chlorophyll containing elements from vegetation.

$$rdNBR = \frac{NBR_{prefire} - NBR_{postfire}}{\sqrt{abs(NBR_{prefire})}}$$

Equation 8 – Relative differenced normalised burn ratio

The relativizing method has been shown to align classes of dNBR between vegetation types differing in spectral density, in terms of NIR and SWIR. This was evident in the Big-Desert image where dNBR values were scaled up relative to the more vegetated sites. Thresholds for burnt pixels were based on visual inspection and literature (Equation 9) (Ireland and Petropoulos, 2015).

$$pixel_{fire} = 5th\ percentile < rdNBR_{pixel}$$

and

$$pixel_{nofire} = -2nd\ percentile < rdNBR_{pixel} < 2nd\ percentile$$

Equation 9 – Burnt sample separation using rdNBR.

No fire measures of rdNBR generally appear as very small positive and negative values, where changes in NIR and SWIR may just be seasonal structure fluctuations (Walz et al., 2007; Lutes et al., 2006). A threshold for control pixels was set at less than or more than ± 2nd percentile of positive values, respectively, based on comparison of low scoring pixels within and without fire scar (Equation 9). Low and high severity pixels were chosen from separate parts of the rdNBR distribution based on values within the fire scar of each site (Equation 10).

$$pixel_{lowsev} = 10th\ percentile \leq rdNBR_{pixel} \leq 15th\ percentile$$

and

$$pixel_{highsev} = 90th\ percentile \leq rdNBR_{pixel} \leq 95th\ percentile$$

Equation 10 - Burn severity classification using rdNBR.

This discrete classification ensures sample pixels represent part of the overall class of interest, without risking misclassifying pixel values that border ascribed class boundaries, particularly between sites, where vegetation is structurally different. Bennett *et al*. (2016) used the same logic. rdNBR along with other remotely sensed fire severity measures have been shown to misclassify when crowns of ecosystems remain intact (Collins et al., 2018). This is a common problem where the upper layer disguises unique spectral features of the affected understory. Values underestimate compared to field based measures. For this study, the boundaries of classes are less important and so the low severity samples allow for underestimation by selection of low rdNBR values in the distribution, and a large buffer to the high severity samples.

An error occurred during severity class processing that was not identified until after outputs had been produced. The fire scar was not applied correctly in coding, and the control pixels were chosen from within the boundary in a minority of cases (<30% for both) at two of the four sites. The rdNBR classification (Equation 10) was applied correctly. Black Saturday and Deua-NP control pixels within the fire scars have values that represent minimal NIR and SWIR change due to fire. Using both the scar and rdNBR in control classing is the preferable approach however the accuracy of rdNBR alone has been shown elsewhere (Parks *et al*., 2014), and accuracy of fire scar origin may vary regardless (5.4.5, p.27). High and low severity classification was unaffected.

5.4.4 Vegetation Classes

Vegetation classes were drawn from the National Vegetation Information System (NVIS) that provides major subgroups of dominant vegetation across Australia at 100m spatial resolution (NVIS Technical Working Group, 2017). The grid for each site was resampled in GDAL and python to the MODIS 0.005^{o} resolution. Each target pixel was taken to be the average of contributing pixels. Based on NVIS metadata the uncertainty associated with age, origin and spatial mix were all low or very low, and scale was highly uncertain for area of the Brindabella site occurring in NSW, and low or very low elsewhere. The vegetation types were visually checked against satellite imagery for major classification errors.

Table 4 - Vegetation classes of sites (NVIS).

Brindabella	% fire scar
Eucalyptus woodlands with a tussock grass understorey	45
Eucalyptus tall open forests and open forests with ferns, herbs, sedges, rushes or wet tussock grasses	38.5
Eucalyptus woodlands with ferns, herbs, sedges, rushes or wet tussock grassland	13.3
Eucalyptus tall open forest with a fine-leaved shrubby understorey	<1
Eucalyptus (+/- tall) open forest with a dense broad-leaved and/or tree-fern understorey (wet sclerophyll)	<1
Eucalyptus open forests with a shrubby understorey	<1

Eucalyptus woodlands with a shrubby understorey	<1
Eucalyptus open forests with a grassy understorey	<1
Wet tussock grassland with herbs, sedges or rushes, herblands or ferns	<1
Wet tussock grassland with herbs, sedges or rushes, herblands or ferns	<1
Heathlands	<1
Other tussock grasslands	<1
Cleared, non-native vegetation, buildings	<1
Black Saturday	
Eucalyptus tall open forests and open forests with ferns, herbs, sedges, rushes or wet tussock grasses	52
Eucalyptus (+/- tall) open forest with a dense broad-leaved and/or tree-fern understorey (wet sclerophyll)	22.4
Cleared, non-native vegetation, buildings	12
Eucalyptus open forests with a shrubby understorey	6
Eucalyptus woodlands with a tussock grass understorey	5
Cool temperate rainforest	<1
Eucalyptus low open woodlands with a shrubby understorey	<1
Other Acacia tall open shrublands and [tall] shrublands	<1
Big-Desert	
Mallee with a dense shrubby understorey	67.5
Heathlands	24.3
Mallee with an open shrubby understorey	4.6
Mallee with hummock grass	3
Eucalyptus woodlands with a shrubby understorey	<1
Deua-NP	
Eucalyptus woodlands with a tussock grass understorey	45
Eucalyptus tall open forests and open forests with ferns, herbs, sedges, rushes or wet tussock grasses	38.5
Eucalyptus woodlands with ferns, herbs, sedges, rushes or wet tussock grassland	13
Other Acacia forests and woodlands	1.8
Warm temperate rainforest	<1
Cleared, non-native vegetation, buildings	<1

5.4.5 Fire scar area

Bushfire scars were based on fire history databases maintained by the relevant government authority (Table 3) (Yebra, 2018). Any inaccuracies are unable to be compensated for due to the historic nature of the datasets, and a wide range of collection techniques.

5.5 Statistical analyses

GPP of all pixels and timestamps were subset spatially using Python libraries. A time series analysis was undertaken in JMP, using one-way ANOVAs and Student t-tests to look between

individual means (SAS Institute Inc., 2007). Local data filters were applied with various month since fire windows.

Cumulative GPP measures were calculated from the time series of different sites and severities. Simpsons rule integration was used, and odd intervals were averaged from the first and last samples. The integrals were subtracted from the control integral to give a quantity of change in primary production. This assumes that GPP of different severities would have the same rate of change through time, if not for the fire. Then the 12 month pre-fire mean GPP of the whole fire scar for each site was used to scale the difference of integrals. The resulting relative quantity shows the lost potential productivity due to fire.

Chapter 6: Results

6.1 Severity and GPP recovery

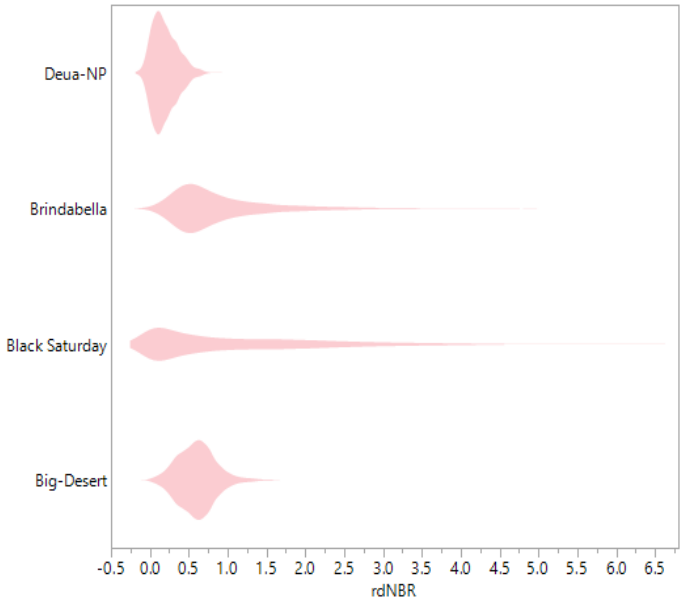

Figure 10 - Contour violin plot of severity (rdNBR) of vegetation, fire effects at each site. Area of each violin is weighted by number of observations at that site.

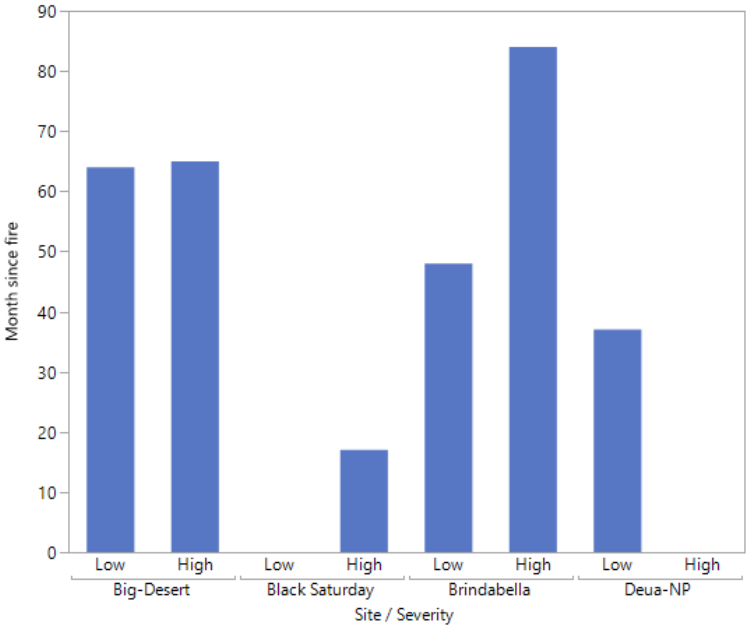

Figure 11 - Months to recovery for different severity classes at each site (all pixels of class). Recovery based on monthly means returning to control means (not shown) for that severity ($p<0.05$). Empty values indicate severities that did not differ from control after fire (Black Saturday) or never returned to control in available data(Deua-NP).

6.1.1 Cross site severity class recovery

The diagnostic GPP model applied here on a fire scar scale showed trends with varying severity between and within 3 sites. At these sites low and high severity GPP pixels recovered at different times (Figure 11). This was based on difference to control, monthly means, and 12 month viewing windows. At Deua-NP, low severity samples recovered GPP at ~50 months, while high severity had not recovered at 14 years following disturbance (data extent). Black-Saturday recovery was different between severity classes, ~20 for high, and low severity GPP did not vary from control. Brindabella, low severity GPP recovered in 48 months, whereas high severity > 80 months. Big-Desert severity classes recovered at the same time (~64 months). GPP of Big-Desert is lower overall (Figure 12), reflecting the semi-arid, shrub land environment (Figure 5). There is a distinct seasonality in GPP, with late summer peaks common (Figure 12).

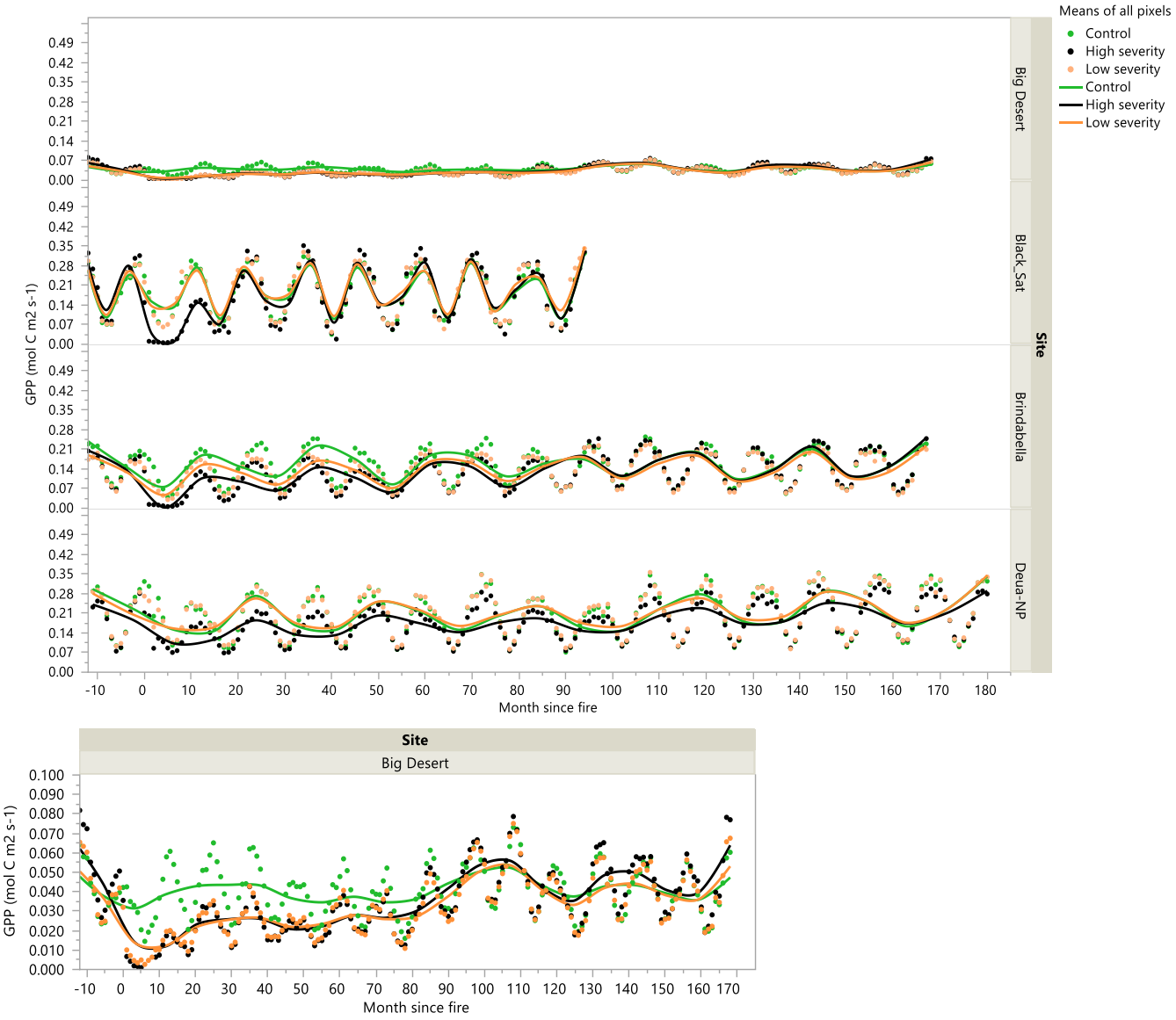

Figure 12 - GPP trends beginning 12 months before fire in two severity classes (high and low) across 4 study fire sites in SE Australia. Points are means of all pixels in associated severity class, trend lines are lambda smoothed. Big Desert is shown separately to enlarge the smaller range of GPP values.

6.1.2 Black Saturday severity class recovery

Black-Saturday generally experienced large differences in productivity for the first year after fire, between severity classes, and converged with control at ~20 months post-fire (Figure 12). High severity areas established a higher than control mean GPP rate (+7.5%) by the end of summer ~24 months after fire. This trend continued for the rest of the time series, significantly so for the 48-72 month period (p=0.0012 - 0.0169), annual mean GPP peaking ~84 months (+12.3% over control). Low severity samples were no different to high severity GPP, after ~24 months post-fire. GPP of low severity also fluctuated from control over the remaining time series.

6.1.3 Brindabella severity class recovery

Brindabella experienced a consistent trend in GPP recovery (Figure 12), where the values corresponding to low severity were positive compared to high severity (i.e. +24% at 30 months and +21.9% at 70 months) and negative to control (Figure 12). GPP of low severity returned to control ~40 months earlier than that of high severity (Figure 11). However some negative fluctuation from control GPP occurred in seasons following. Post-recovery coupling of GPP in all severity classes was strong for the remaining data.

6.1.4 Big-Desert severity class recovery

GPP of low and high severity vegetation were different to control for the year following fire (both p=<.0001), although there was no difference between the severity classes themselves (p=0.9256) (Figure 12). This relationship to control was no longer significantly different ~65 months post-fire (p>0.05), for both classes (Figure 11). ~48 months later there was some positive fluctuation of high severity vegetation mean GPP (4%) from control, which was different to low-severity as well (p=<.0001).

6.1.5 Deua-NP severity recovery

The low severity samples of GPP showed no significant difference to control in the 11 months before fire, whereas high severity samples did during this period (Figure 12). This decoupling of high severity GPP persisted after the fire and through the rest of the time-series (mean -27% control GPP, p=<.0001). However, low and control sample GPP were also significantly different for this period (-7% control, p=<.0001). The GPP of low severity samples recovered to control means, first at 30-40 months post-fire, however there was negative fluctuation over the next 36 months.

6.1.6 Severity class to control variation across sites

The pre-fire GPP of control samples were no different to pre-fire low severity at Big-Desert and Black Saturday. At these sites the high severity samples were significantly different for at least 12 months prior (p<0.05). Brindabella and Deua-NP showed no difference between all GPP

samples pre-fire. These statistics are limited in their explanation due to the possibility of inter-annual variability.

6.1.7 Within severity class comparison across sites

Analysing severity class GPP recovery between sites for all comparable data (94 months post-fire); Black Saturday and Deua were similar in high and low GPP classes respectively (p=0.946) (Figure 11). Brindabella and Deua-NP also had GPP means no different to each other for low and high severity classes respectively, during 94 months after disturbance.

6.1.8 Cumulative GPP of severity classes across sites

Figure 13 shows the integral of mean GPP, for low severity, high severity and whole fire scar, less the integral of mean GPP of control, through 94 months after fire. Values were scaled using mean pre-fire GPP for each site and class. This provides a relative quantity of potential lost productivity for each severity sample, if the fire had not occurred. Black-Saturday had a relatively small cumulative loss of GPP in high severity pixels. Big-Desert had a large lost potential productivity across severity classes.

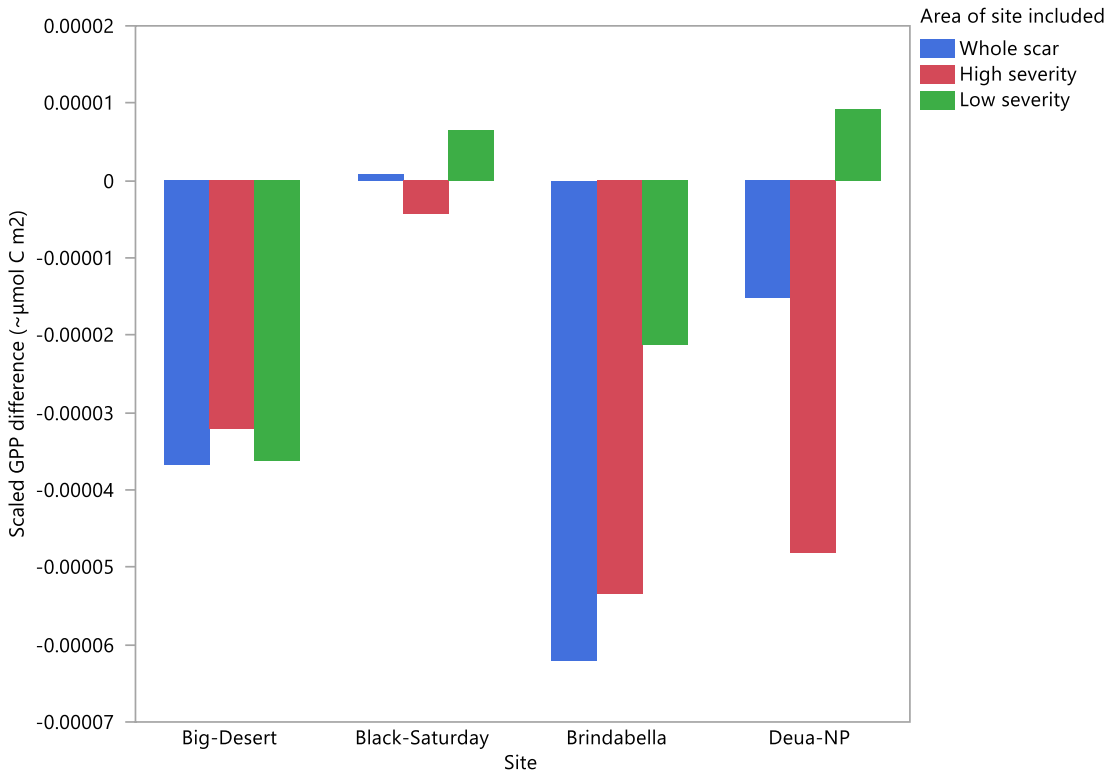

Figure 13 – Scaled cumulative GPP difference over 8 years following fire. Difference is the integral through time of each severity class less the control integral. Values are scaled based on the pre-fire mean at respective sites to give relative change across sites.

6.2 Vegetation class and GPP recovery

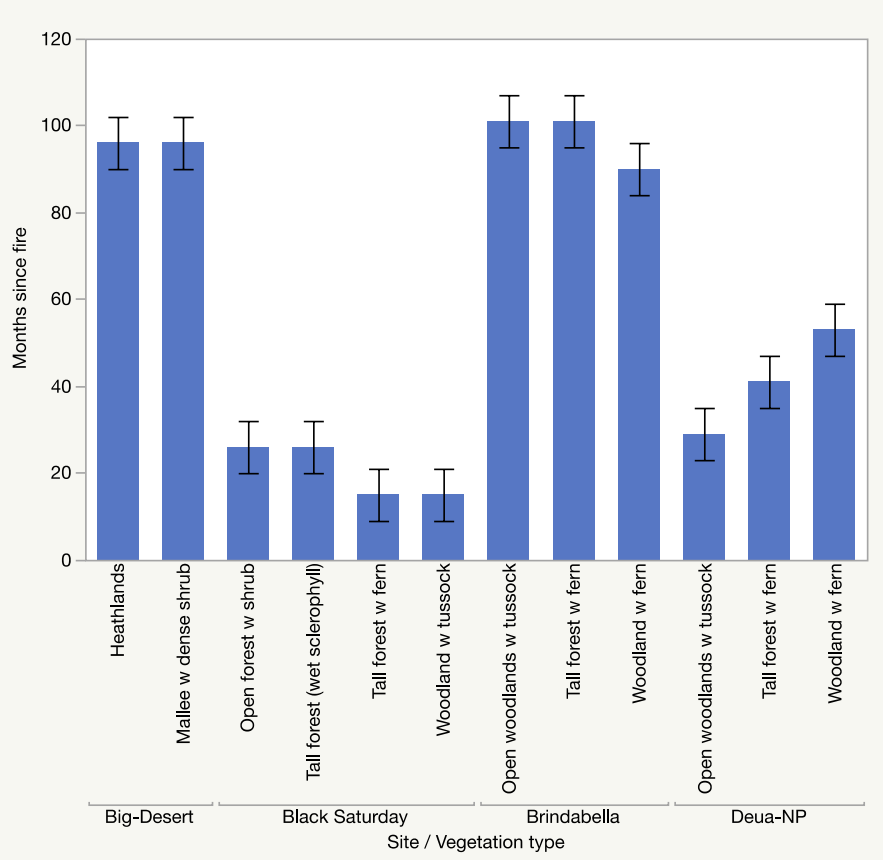

Figure 14 - Months to recovery for major vegetation classes at each study fire, including all pixels of respective class in the burnt area. Minor vegetation classes are < 10% of fire scar and are not shown. Recovery is the time at which a given vegetation class is not significantly different to control ($p<0.05$) for 12 months. Error bars indicate the 12 months during which the class recovered.

GPP recovery time varied between vegetation classes in three of four study sites (Figure 14). Recovery is the number of 12 month periods where means of each class differed from a control of the same class that was unaffected by fire. Sites, except Big-Desert, had a pattern of sequential between class recoveries. However, the major classes (> 10% of fire scar) tended to be closer in GPP recovery times (Figure 14, minor classes not shown). For the same vegetation class across sites there were large differences (see 6.3, following). At Black-Saturday all vegetation types had GPP no different to control 24-36 months after fire.

6.3 Vegetation and severity, and GPP recovery

6.3.1 Overall highest and lowest mean GPP of sub-classes

Warm temperate rainforest that experienced low-severity fire at Deua-NP was the most productive severity-vegetation sample (mean 2001-2016) (Figure 15). A similar overall GPP (mean 2008-2016) occurred at Black-Saturday in tall shrub lands/open shrub lands where burnt to low-severity (Figure 15).

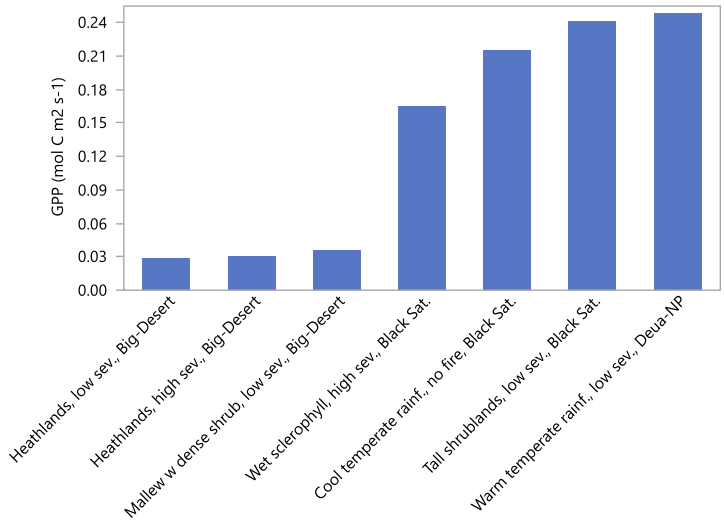

Figure 15 - Highest and lowest mean GPP vegetation-severity sub-samples from all available data (for relevant site)

6.3.2 Range of vegetation-severity samples across sites

Brindabella had the highest frequency of vegetation GPP classes (n=12), as well as the most vegetation-severity GPP classes, with 17 different means classes in the 3rd post-fire year. These included low severity, high severity, whole fire scar or control. Many of these vegetation-severity classes constitute minor landscape cover classes. The range of mean GPP, at Brindabella, between the highest and lowest vegetation-severity sample was 137% between non-native vegetation (pasture) and open forests with grassy under storey (all comparable data). Over the full-time series, at Black Saturday, GPP of open forests and low open woodlands with shrub control samples were no different than burnt equivalents.

6.3.3 Before/after comparison across all severity-vegetation classes

GPP recovery across classes was characterised by a negative shift in values at Big-Desert and an increase in highly positive values at Black-Saturday (Figure 16).

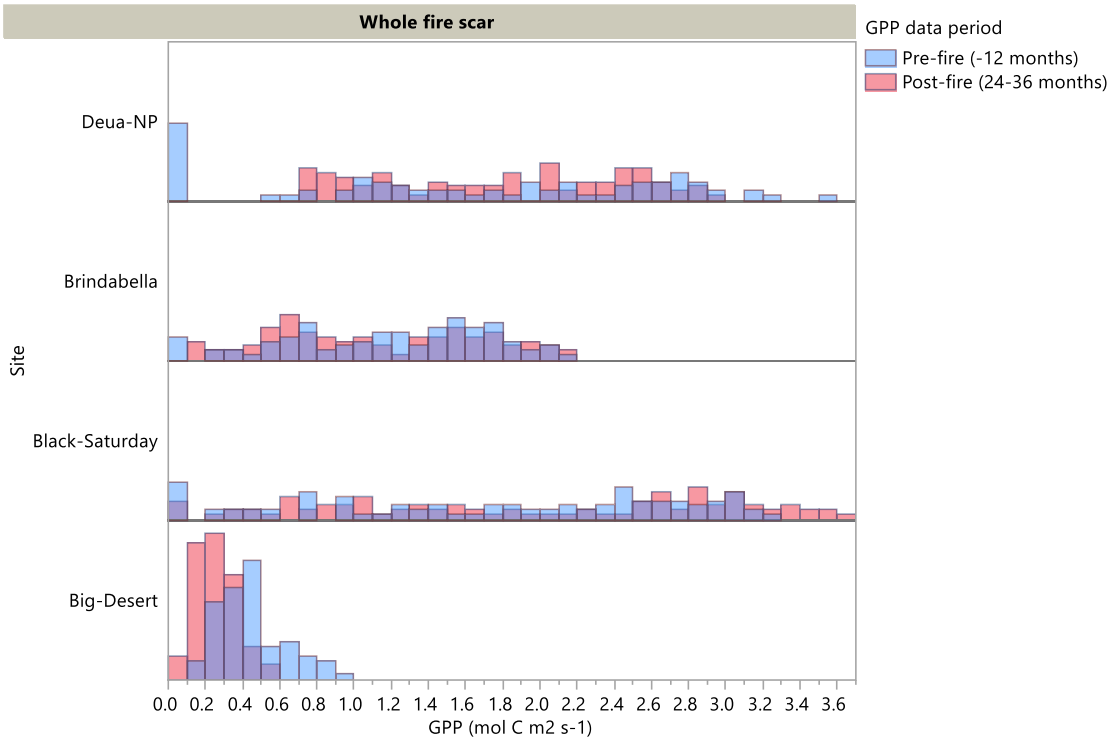

Figure 16 - Distribution of GPP at each site prior to fire and in the third year post fire. Data is the mean of all fire scar pixels, including all severity classes.

6.3.4 GPP recovery in dominant vegetation class at high severity

Black Saturday site showed a short recovery trend in major vegetation types (Figure 17a), particularly those burnt to high severity. Similar vegetation-severity classes at Brindabella (i.e. high severity, tall forest with fern) recovered more gradually and this applied for other classes (Figure 17b). While high severity samples at Deua-NP did not recover overall (Figure 11 and Figure 12), the less productive woodlands and the tall forests (of high severity) recovered within the time series (Figure 18c).

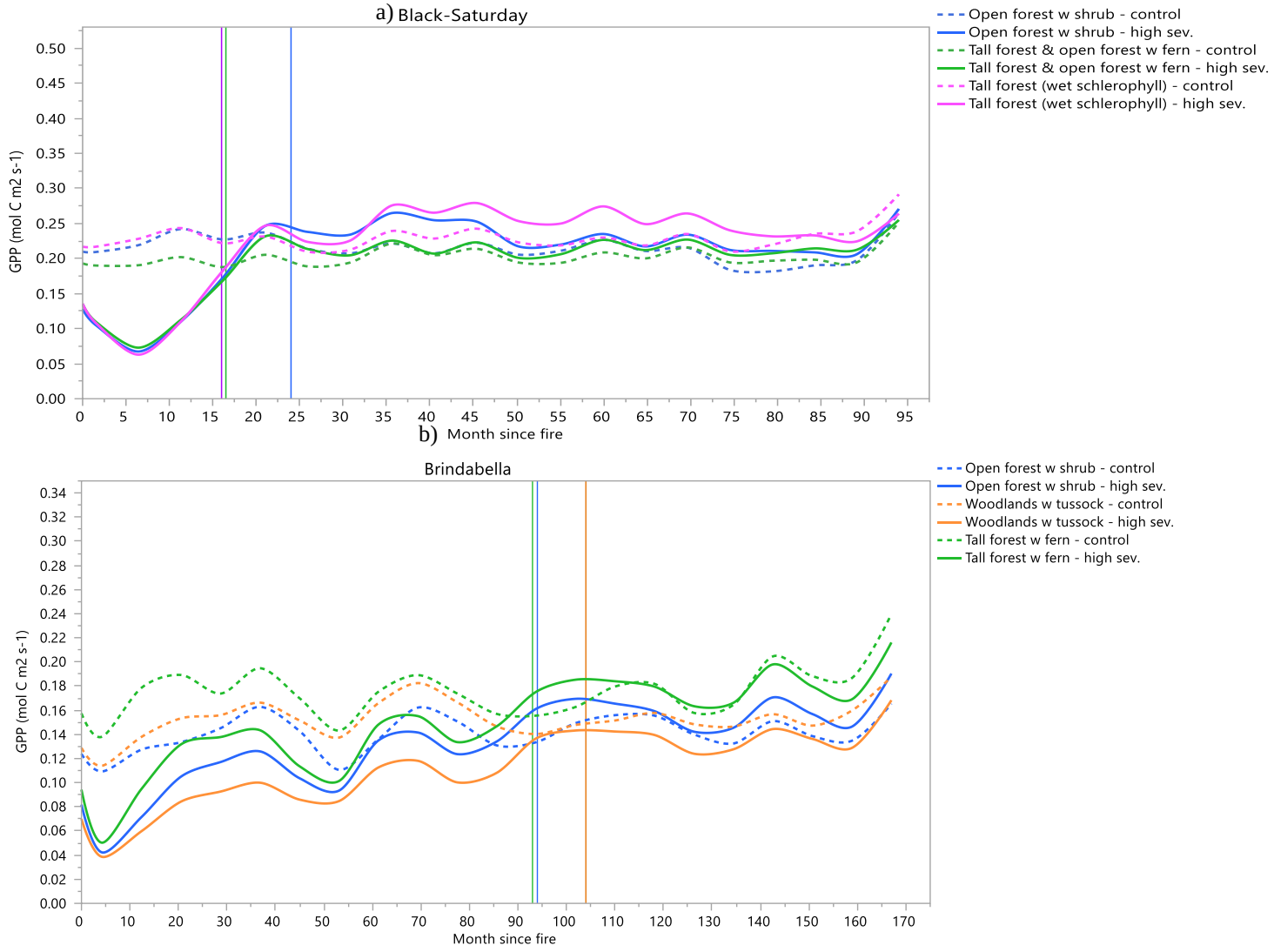

Figure 17 - Recovery of GPP for major vegetation types within sites. Only lambda smoothed mean time series shown (the delay in minimum GPP after month 0 is due to this smoothing not delay in data). Vertical lines reference the time at which recovery to control occur.

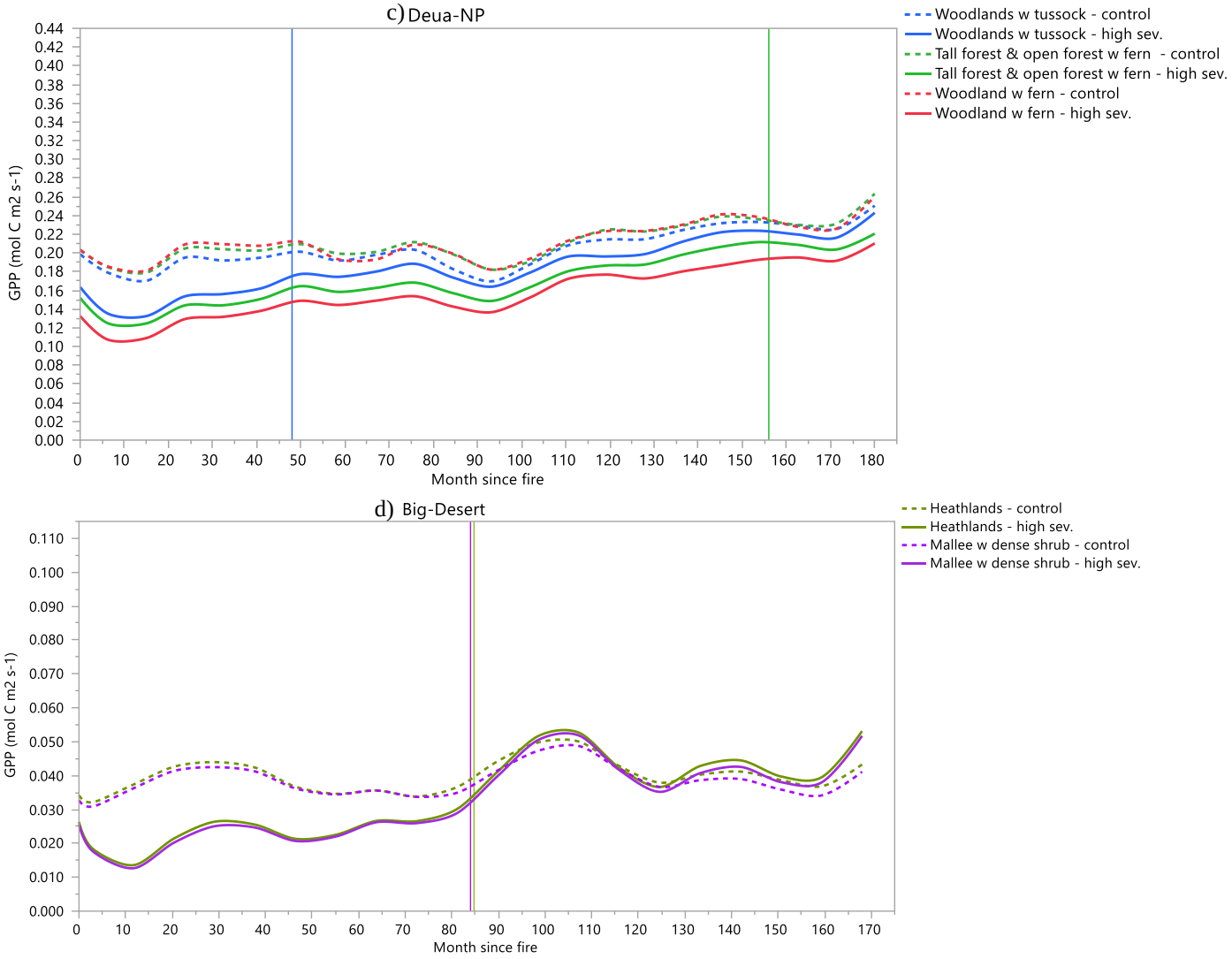

Figure 18 - Recovery of GPP for major vegetation types within sites. Only lambda smoothed mean time series shown (the delay in minimum GPP after month 0 is due to this smoothing not delay in data). Vertical lines reference the time at which recovery to control occur.

6.3.5 Recovery trends of high-severity, dominant-vegetation classes

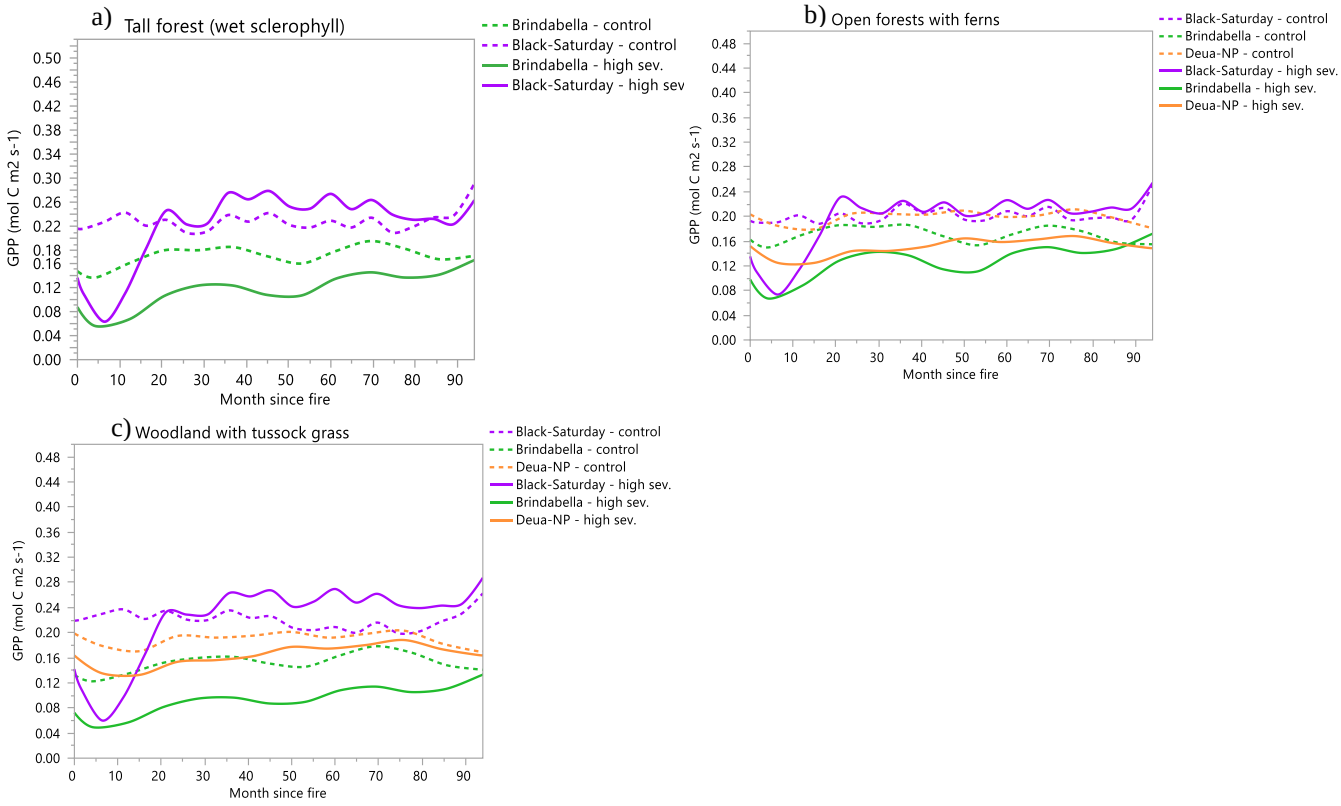

Figure 19 - GPP recovery of three vegetation classes at the three sites where they occurred (Brindabella: green, Black-Saturday: purple, Deua-NP: orange). Dashed lines represent control samples, solid lines high severity.

6.3.6 GPP recovery of Wet sclerophyll forest (Figure 19a)

Wet sclerophyll forest recovered differently between sites Brindabella and Black Saturday (Figure 19a). In high severity samples, the immediate GPP loss was relatively more from fire at Black Saturday (~3% difference pre-fire and fire year means) followed by a rapid increase (no different to control in 12-24 months post-fire ($p=0.7911$, Figure 19a).

6.3.7 GPP recovery of Eucalyptus tall open forests/open with ferns (Figure 19b)

GPP recovery of Eucalyptus tall open forests/open forests with ferns, herbs, sedges, rushes or wet tussock grasses is shown in Figure 19b. The GPP of low severity samples across 3 sites recovered in 2nd year post-fire. High severity was similar to control GPP in the 72-84 months after fire and was no different the following 12 months ($p=0.1888$). This gradual GPP recovery with time is due to relatively longer recovery of the vegetation class in high severity samples at Deua-NP and Brindabella sites (Figure 17). At Black-Saturday in high severity, tall forests rapidly recovered similar to Wet sclerophyll trends. There was no difference in GPP between the tall forests class across the 3 sites, in which they were present, for 12 months pre-fire.

6.3.8 GPP recovery of Woodland with tussock grass (Figure 19c)

In Open woodland with tussock grass under storey of high severity, the GPP was recovered at Black-Saturday but not Brindabella in the seventh year after fire (Figure 19a and Figure 18c). Over this period, the high severity class of the open woodland with tussock became more productive than low severity at all sites, except Deua-NP. However, the trend suggests that high would have surpassed low severity GPP in 12 to 24 months after (2017/18) available data finished.

Chapter 7: Discussion

RS diagnostic GPP modelling is capable of tracking landscape recovery from fire. As well as differentiating vegetation sub-group response to varying fire severity. There was a positive trend in all vegetation classes and severities with time after fire. Overall variation between sites is expected as landscapes have different productive capacity across Australia (Keith et al., 2010). They also tend to recover differently from fire depending on many factors, a few of which are characterised in the results. Big-Desert fire site showed a consistent GPP recovery trend across and within severity and vegetation types. Conversely, rapid recovery observed at Black-Saturday is likely due to a regeneration strategy in the major vegetation classes, present in the area. Slower recovery at other sites may exemplify a different, fire tolerant regeneration strategy. Cumulative GPP changes showed a substantial impact on Big-Desert relative to pre-fire rates and other sites. Also, samples across sites had varying representativeness depending on landscape cover. Overall the GPP model could be refined per-site to better discern dynamic time series of all vegetation-severity sub-classes in response to fire.

7.1 The difference at Big-Desert

Analysing the Big-Desert site led to the rejection of the hypothesis that GPP recovery is dependent on vegetation type. Modelled GPP of all NVIS vegetation classes within the fire scar returned to control at the same time (Figure 14). Classes responded similarly through time and were no different across major vegetation types before or after fire (any time window). This small GPP range across and within vegetation classes was unable to explain variation in recovery. The rdNBR at Big-Desert had a relatively high mean and smaller distribution than the other sites (Figure 10). rdNBR is an index that measures change over the disturbance period and also considers the pre-fire vegetation condition. Consequently the index can be compared between sites (Parks, *et al.*, 2014). Therefore, fire affected all vegetative pixels to a more consistent, higher degree at Big-Desert relative to other fires. The distribution of average GPP was also small although low, before the fire, compared to other sites (Figure 16). Observed similarity in recovery time between classes (Figure 11) is partly due to a highly destructive fire, consistently burning a landscape that had small spatial gradients of GPP across and within vegetation types. Severe bushfire has shown to strongly affect heathland structure, between different sites of the same event (Foster et al., 2017). Also, time since disturbance has been shown to drive changes in vegetation structure (Kenny et al., 2018) and may be more important than vegetation class effects on GPP recovery time in the Big-Desert Mallee/heathland environment.

The other hypothesis stated that, GPP recovery time is dependent on fire severity. Again at Big-Desert, the two severity classes tested showed the same recovery time. Hence the hypothesis was rejected. Vegetation classes within severity classes also showed the same trends to recovery.

No difference between GPP of low and high severity, within any vegetation class, was seen for any 12 month window following disturbance. However, before fire there was a difference in GPP between low and high severity of the major vegetation classes. A difference in one minor vegetation cover also occurred. Therefore overall, the two severity class samples had different GPP rates in the 12 months before fire ($p=0.0038$). This difference did not last through disturbance. The complete simplification of GPP composition, within vegetation-severity classes, due to the fire event, is not seen at other sites. It indicates the strong impact of fire on landscape function at this site.

The association of areas of vegetation affected to high severity with areas of elevated pre-fire GPP is due to unique fire regime characteristics at this site. Assuming that the GPP values observed 12 months pre-fire are representative of vegetation classes historically, the fire was highly affective in more productive (higher GPP) vegetation. This is likely due to preference for fire to burn where there is more stored GPP through time (e.g. more fuel load). Contrastingly, at Deua-NP and Brindabella areas that didn't burn or burnt to low severity were higher in productivity before disturbance than high severity samples. The trend at Big-Desert suggests that fire prefers to burn areas with high productivity. This observation supports the theory, of mallee-heath shrubland, that "conditions required to support fire spread will lead to crown fire propagation and high rates of spread" (Cruz et al., 2013). Analysing fuel loads and burnt area in this environment may reflect these observations of GPP accumulation.

Lack of differentiation between GPP values of different vegetation classes occurred after the Big-Desert event. The study period may have been too short to capture the establishment of tree type over store, hence the slow spatially consistent recovery. Slow growth is characteristic of over storey species at this site. Also, species present require large fire intervals to regenerate from seed (National Parks Service and Department of Conservation and Natural Resources, 1994). Other areas of the site have seen a change in composition with fire because of this immature age composition. Notable changes include a reduction in dominant Scrub pine woodland including a loss of co-dominants, Desert Banksia and Dwarf She-oak, and an increase in annual lifecycle species in the understorey. The fire regime at this site has been classified as, infrequent medium intensity shrub fires in spring and summer (Murphy et al., 2013). Given high intensity fire events have occurred in 1959 and 1985 (also moderate severity fires in 1991 & 1999), there may be an increasing high intensity fire frequency which is reducing the viability of canopy dominant, seed regenerating species (Land Conservation Council, 1987). The low and spatially consistent post-fire GPP across the fire scar supports these observations. A loss of indigenous tree species and canopy establishment of fire tolerant shrub species is a possible explanation.

The Big-Desert GPP composition and recovery was strongly impacted by a high severity event. The distribution of GPP within and across severities indicates that fire completely disrupts landscape productivity. This may be explained by changing fire regime and fuel accumulation dynamics.

7.2 Black Saturday rapid recovery

Both severity and vegetation class affect GPP recovery at the Black Saturday. This recovery occurred rapidly in major vegetation classes (> 10% of fire scar). Fastest response occurred in high severity samples. The model responded to the increased area of leaf photosynthetic components, via increasing VI derived fPAR (Donohue *et al*., 2008) and stomatal conductance (Yebra et al., 2013b). The vegetation most responsive to this change was tall and open forests, and wet sclerophyll. In high severity classes this is likely due to canopy mortality and subsequent stand replacement. Mountain Ash and associated communities, regenerate in this way (Brookhouse *et al.*, 2013). Additionally 10% of the site was covered with locally sourced seed via helicopter within 6 months of fire (Department of Sustainability and Environment, 2012). This enhanced the GPP recovery time observed here. Growth to canopy closure occurs in 1.5 to 5 years in naturally regenerating forests (Polglase and Attiwill, 1992). This aligns with the timeframe of recovery and maximum GPP modelled here (~24 months depending on class). Modelled GPP responded quickly with rapid increase of photosynthetically active area after fire in a mesic, stand-replacement landscape.

Modelled GPP explicitly includes canopy conductance to CO_2, via H_2O coupling in the stomata. This mechanism drives modelled GPP in Ash forests during the growing season due to high temperature (Figure 5) and associated vapour pressure deficit (time series in Appendix 1), Therefore positive recovery trends are estimated mostly by conductance driven GPP. Buckley *et al.* (2012) found that stomatal conductance of Alpine Ash was ~200% that of mature forest three and four years after severe bushfire, increasing the landscape water use. In this study, over the same period, GPP rates of tall, high severity forests had significantly higher total GPP than the control samples. Therefore the conductance driven modelling represents GPP through time well compared to other research. This conductance characteristic of the major vegetation class may be a better representation of GPP than radiation, or leaf area, during stand replacement. Buckley *et al.* (2012) also found that there was no difference in photosynthetic capacity between leaves of control and regrowth plots of 3 years. The importance of conductance driven GPP is less after this photosynthetic capacity is restored as radiation driven estimation has become more accurate. Given this short restoration, uncertainty of GPP at Black-Saturday is reduced to only a few years post-fire. This was not explicitly tested here and the GPP model inherently relies on the canopy productive area estimates of VIs. However modelled GPP, when driven by conductance, does not rely on the time averaged estimate of photosynthetic capacity (i.e. ε, **Equation 1**). There is good evidence showing that time averaged ε, over predicts GPP due to changing photosynthetic capacity with stand age (e.g. Cheng *et al.*, 2006). In this study, the effect may be reduced due to rapid leaf expansion and action of the canopy conductance component.

7.3 Slower recovery

GPP particularly of high severity classes recovered more slowly at Deua-NP and Brindabella. This is likely due to mixed canopy survival and mortality. The distribution of GPP values at 24-36 months post-fire, within high severity, particularly forest vegetation, classes tend to be lower than pre-fire values. GPP regrowth in majority forests at Brindabella and Deua-NP are characteristic of stand survival and epicormic regeneration strategy (Nicolle, 2006). After fire individuals slowly, relative to stand replacement, regrow into new niches and establish lost structure (Pausas and Keeley, 2014). A slow increase in VI values due to this regeneration is captured by both model components. There is a small portion of the site that likely uses reseeding regeneration (Vivian et al., 2008). However the extent is reduced compared to the Black-Saturday site. Also, severities were not high enough (Figure 10) to cause large scale canopy loss and stand replacement, at Deua-NP. Furthermore, Brindabella and Deua-NP have high EVI values (Figure 7 and Figure 9), indicating structurally complex canopies (Huete et al., 2002). The productive leaf area of regrowth maybe hidden in complex canopy structures where reflectance below the canopy is not measured (e.g. Palace et al., 2015). If this is the case fPAR and G_{cw} may be underestimates, and this would explain the gradual increase of GPP in classes that may be expected to respond more quickly (i.e. Figure 19a). Alternately the forest structure combusted is gradually replaced by regrowth of photosynthetically productive area, resulting in higher VI values in the long term. The modelled GPP uses a combination of indices that differentiate complex vegetation, more (Polychronaki *et al.*, 2014) or less well. For instance EVI deals well with complexity and background signals (Huete et al., 2002). GPP trends of mixed age forest regeneration and regrowth of individuals are captured in the recovery time series.

At Deua-NP, high severity class overall vegetation types, did not recover during the studied period (14 years post-fire) (Figure 11). However some major (> 10% fire scar cover) and minor vegetation-high severity classes did return to control (Figure 18c). Major vegetation classes therefore respond with a wide range of recovery times for the same severity class. This range of responses occurred after an event with relatively low severity compared to other sites (Figure 10). Woodland with fern under storey (third largest vegetation class) of high severity had a GPP that was significantly negative to control and low severity before the fire (22 months, p=0.0002) and remained lower throughout the post-fire period. Other high severity vegetation classes did not show this consistent decoupling. This high severity class covers ~13% of the fire scar resulting in small sample sizes per timestamp (mean=0.89 pixels). However sample size is smaller in the low severity class, which did not have an anomalous recovery. This vegetation class is mostly distributed along ridgelines in linear patterns between other dominant vegetation classes. The anomaly of high severity GPP may be due to mixing of pixels when average rescaling was applied. 500m resolution is large compared to the environmental niches this vegetation classification prefers. While modelling disturbance scales using MODIS resolution data is

effective (Buma, 2012; Di Mauro et al., 2014) analysing features therein that comprise single, dispersed pixels may reduce accuracy.

7.4 Productivity losses after fire

There was a relatively large cumulative GPP loss at Big-Desert compared to other sites when values were scaled using pre-fire GPP of each site (Figure 13). The largest loss of potential stored carbon and respiration overall was at Brindabella, without considering relative size of fire scar. Areas of high severity at this site experienced the largest loss, as is expected with canopy consumption and mortality (Hicke et al., 2003). This cumulative GPP measure is assumed to be indicative of NPP (i.e. stored carbon) in the landscape. NPP is GPP less heterotrophic respiration, which varies within a limited range for a given vegetation class (Verma et al., 2017). High temporal resolution allowed quantification of consistent GPP time series across sites and within severity classes. This model driven quantification of GPP highlights relative effects of fire on potential NPP and carbon stocks. Further analysis of cumulative GPP of vegetation-severity subsamples may reveal stand scale areas of loss. However pixel size to target ratios may limit vegetation-severity sample representativeness (Jensen, 2007). Brindabella had the largest loss of potential stored GPP across severity samples.

Potential NPP loss at Big-Desert was substantial and is due to a slow GPP recovery in all vegetation and severity classes. This contrasts the ostensible biomass consumption in woodlands or forests of the other sites. There was a minor difference through time between cumulative low and high severity class GPP at Big-Desert. Relatively large production potential (cumulative GPP) loss emphasises heath/shrub-land inability to quickly return to pre-fire vegetation vigour within timeframes of decades. Further field testing could indicate if vegetation classification has changed after this fire, in light of an increasing fire regime (Esplin *et al.*, 2003). As previously described, the model shows unequal reductions in severity classes of different GPP means before fire and equal recovery trends post-fire. This indicates vegetation in the fire scar shifted GPP means classes in the long-term. The simplistic landscape scale response to high level disturbance is likely due to a change in composition of vegetation involving slow growing species. Long term cumulative GPP loss, results in NPP loss through time and ultimately reduction in fixed woody carbon matter.

Low severity GPP samples studied, particularly at Black-Saturday and Deua-NP (Figure 11) had capacity to maintain carbon capture across the disturbance period. Many forested, predominantly *Eucalyptus*, landscapes of SE Australia maintain this tolerance (Bennett et al., 2016). A net gain in productive potential over 8 years since fire indicates an initial landscape process loss was made up for by regeneration. This is likely due to fire tolerant regrowth strategies, mentioned earlier. Brindabella lost growth potential in low severity, however this was less than half that of high severity sample loss. Low severity GPP recovery times were most different to control (negative) and high (positive) severity samples' GPP at this site compared to

other sites (Figure 11). Therefore low severity vegetation was more highly impacted at Brindabella than other sites and led to a net loss of cumulative GPP over 8 years. Classification of severity may be part of the explanation, where low severity pixels of other sites are closer to control values. A range of low severity class GPP response indicates the variability in vegetation response with severity effects.

7.5 Microscale effects on severity samples

As previously mentioned, Big-Desert GPP differed between severity classes prior to disturbance. This was the case at the other sites to a lesser degree. Ideally pre-treatment values do not vary across groups, however this is an effect of using a concurrent control sample. The variation represents spatial gradients in productivity, where stratification of pixels for vegetation type and proximity to fire may not account for other local environmental factors. Such landscape scale factors, like slope, aspect and moisture availability will affect GPP (Potter et al., 1993). Such micro-environments may cause the observed pre-fire fluctuation. Averaging a control sample out of pre-fire severity classes was considered, although cross-class factors would then be different through time. The use of stratified control pixels allows environmental factors to vary across all GPP groups through time (Di Mauro et al., 2014). Drought had effect on much of SE Australia for 2001-2010 period. This type of variance is accounted for in the change detection approach used here. Also the increase in atmospheric CO_2 due to anthropogenic pollutants (Beer et al., 2010) has a fertilising effect on vegetation (Haverd et al., 2013). Using local, concurrent control pixels, removes uncertainty of this background variation. Discrepancies in pre-fire sample groups is the result of spatially explicit control sampling in a heterogeneous landscape.

7.6 Model assessment

The recovery of GPP between and within sites suggest there are some limitations to its application for fire assessment. Without field checking, these cannot be explicitly examined. The GPP model captured significant variation with fire effects. The conductance component was the limiting factor in hot dry summers (Appendix 1). It tended to have an earlier and lower seasonal peak than the radiation component. The difference is due to the contribution of humidity deficit limitation on conductance, the assumption being increased radiation does not always increase GPP (Yebra et al., 2015). The slow recovery at Brindabella and Deua-NP is partly explained by this relationship. A combination of factors occurs at these sites; a loss of leaf area in mixed age regrowth slowly increases productive area estimates (i.e. VIs). The second factor is conductance limitation during the growing season. Ultimately the combination lowers the maximum GPP each year during recovery, extending the recovery period. This feature, generally improves the GPP estimation by reducing the overestimation sometimes present in LUE GPP modelling (Madani et

al., 2014). Maximum light use efficiency will have changed in most sites at least in the short term recovery (e.g. Zhou et al., 2015). Reducing the influence of the LUE component in cases where there is varying maximum light use efficiency is considered beneficial.

The authors of the GPP model calibrated at 16 sites globally to derive the parameters used here. Errors of model performance against FLUXNET measurements, were the largest in severely water-limited ecosystems (Yebra et al., 2015). This may have effect on GPP of semi-arid Big-Desert site. Calpernum Station is a FLUXNET site located in similar vegetation, ~200km north of the study site, where validation of the outputs could be undertaken. Further analysis could include the fitting of site specific vegetation indices for each model component. Refining the model this way may increase the range of GPP between landscapes of simple and complex vegetation. For instance, EVI is less suited to a semi-arid, low canopy cover vegetation than NDVI (Huete et al., 2002). The model application and dataset established here have potential for revision and further analysis.

Chapter 8: Conclusions

Landscape scale gross primary productivity is a complex process that is dramatically disturbed by fire. Different vegetation sub-groups and variation in severity cause fluctuation in the capacity of growth after fire. Monthly to yearly fluctuations due to these events are captured by a remotely sensed model, without field observation. Regional scale satellite resolutions, integrating reflectance and meteorological data are used to analyse disturbance in terms of ecosystem processes. This thesis applied a diagnostic GPP model across four bushfires of varying intensity in different fire regimes of temperate south-eastern Australia. GPP of a semi-arid heath-mallee landscape was found to respond uniformly to a high severity bushfire. While other sites in different vegetation varied at high severity. Vegetation sub-groups had little variation in GPP recovery, at Big-Desert. Cumulative loss of GPP was relatively high at this site compared to sites that contain higher structural complexity, like montane forests.

The GPP of vegetation with relatively fast regeneration was captured in moist forests of Victoria, where recovery to unburnt levels was within a few years. The two-part model allowed more subtle response to different physiological drivers, seasonally and during recovery. Vegetation-severity sub-samples of the Black-Saturday forest were faster to respond, where the model captured an increasing canopy conductance and photosynthetic potential. The utility of high temporal resolution of satellites was explored, allowing inter and intra-year comparison of disturbance recovery. Fire severity plays an important role in recovery time and trajectory in sites with complex vegetation structure. In these landscapes GPP of open and grassy vegetation tend to recover a few years before dense closed types. Major vegetation classes at Big-Desert and Brindabella had a long recovery period indicating a relatively large impact on landscape processes.

Fire disturbance of GPP of vegetation is different between landscapes. With frequency of disturbance events likely to increase in coming decades, the analysis of environmental impacts of fire and integration of this fluctuation into subsequent modelling is considered important for environmental assessment.

Chapter 9: References

Andela, N., Liu, Y.Y., M. Van Dijk, A.I.J., De Jeu, R.A.M. and McVicar, T.R., 2013. Global changes in dryland vegetation dynamics (1988-2008) assessed by satellite remote sensing: Comparing a new passive microwave vegetation density record with reflective greenness data. *Biogeosciences*, **10**(10): 6657–6676.

Asrar, G., Fuchs, M., Kanemasu, E.T. and Hatfield, J.L., 1984. Estimating Absorbed Photosynthetic Radiation and Leaf Area Index from Spectral Reflectance in Wheat1. *Agronomy Journal*, **76**: 300–306. Available at: http://dx.doi.org/10.2134/agronj1984.00021962007600020029x.

Bartels, S.F., Chen, H.Y.H., Wulder, M.A. and White, J.C., 2016. Trends in post-disturbance recovery rates of Canada's forests following wildfire and harvest. *Forest Ecology and Management*, **361**: 194–207. Available at: http://dx.doi.org/10.1016/j.foreco.2015.11.015.

Beer, C., Reichstein, M., Tomelleri, E., Clias, P., Jung, M., Carvalhais, N., Rödenbeck, C., Arain, M.A. and Baldocchi, D., 2010. Terrestrial gross carbon dioxide uptake: Global distribution and covariance with climate. *Science*, **239**(August): 834–838.

Bennett, L.T., Bruce, M.J., MacHunter, J., Kohout, M., Tanase, M.A. and Aponte, C., 2016. Mortality and recruitment of fire-tolerant eucalypts as influenced by wildfire severity and recent prescribed fire. *Forest Ecology and Management*, **380**: 107–117. Available at: http://dx.doi.org/10.1016/j.foreco.2016.08.047.

Biswas, S., Lasko, K.D. and Vadrevu, K.P., 2015. Fire Disturbance in Tropical Forests of Myanmar-Analysis Using MODIS Satellite Datasets. *IEEE Journal of Selected Topics in Applied Earth Observations and Remote Sensing*, **8**(5): 2273–2281.

Bowman, D.M.J.S., Balch, J.K., Artaxo, P., Bond, W.J., Carlson, J.M., Cochrane, M.A., D'Antonio, C.M., DeFries, R.S., Doyle, J.C., Harrison, S.P., Johnston, F.H., Keeley, J.E., Krawchuk, M.A., Kull, C.A., Marston, J.B., MaxA.Moritz, Prentice, I.C., Roos, C.I., Scott, A.C., Swetnam, T.W., Werf, G.R. van der and Pyne, S.J., 2009. Fire in the Earth System. *Science*.

Bradstock, R.A., 2010. A biogeographic model of fire regimes in Australia: current and future implications. *Global Ecology and Biogeography*, **19**(2): 145–158. Available at: http://doi.wiley.com/10.1111/j.1466-8238.2009.00512.x.

Brookhouse, M.T., Farquhar, G.D. and Roderick, M.L., 2013. The impact of bushfires on water yield from south-east Australia's ash forests. *Water Resources Research*, **49**(7): 4493–4505.

Buckley, T.N., Turnbull, T.L., Pfautsch, S., Gharun, M. and Adams, M.A., 2012. Differences in water use between mature and post-fire regrowth stands of subalpine Eucalyptus delegatensis R. Baker. *Forest Ecology and Management*, **270**: 1–10. Available at: http://dx.doi.org/10.1016/j.foreco.2012.01.008.

Buma, B., 2012. Evaluating the utility and seasonality of NDVI values for assessing post-disturbance recovery in a subalpine forest. *Environmental Monitoring and Assessment*, **184**(6): 3849–3860.

Cernusak, L.A., Hutley, L.B., Beringer, J. and Tapper, N.J., 2006. Stem and leaf gas exchange and their responses to fire in a north Australian tropical savanna. *Plant, Cell and Environment*, **29**(4): 632–646.

Cheng, Y., Gamon, J.A., Fuentes, D.A., Mao, Z., Sims, D.A., Qiu, H. lie, Claudio, H., Huete, A. and Rahman, A.F., 2006. A multi-scale analysis of dynamic optical signals in a Southern

California chaparral ecosystem: A comparison of field, AVIRIS and MODIS data. *Remote Sensing of Environment*.

Choinski, J.S., Ralph, P. and Eamus, D., 2003. Changes in photosynthesis during leaf expansion in Corymbia gummifera. *Australian Journal of Botany*, **51**(1): 111–118.

Chuvieco, E., 2009. *Earth Observation of Wildland Fires in Mediterranean Ecosystems*. [online] Berlin, Heidelberg: Springer Berlin Heidelberg. Available at: http://link.springer.com/10.1007/978-3-642-01754-4.

Ciais, P., Sabine, C., Bala, G., Bopp, L., Brovkin, V., Canadell, J., Chhabra, A., DeFries, R., Galloway, J., Heimann, M., Jones, C., Quéré, C. Le, Myneni, R.B., Piao, S. and Thornton, P., 2013. Carbon and Other Biogeochemical Cycles. In: S. T.F., D. Qin, G.-K. Plattner, M. Tignor, S.K. Allen, J. Boschung, A. Nauels, Y. Xia, V. Bex and P.M. Midgley, eds., *The Physical Science Basis. Contribution of Working Group I to the Fifth Assessment Report of the Intergovernmental Panel on Climate Change*. Cambridge, United Kingdom and New York, NY, USA: Cambridge University Press, pp.465–570. Available at: http://www.ipcc.ch/report/ar5/wg1/docs/review/WG1AR5_SOD_Ch06_All_Final.pdf%5Cnhttp://ebooks.cambridge.org/ref/id/CBO9781107415324A023.

Clark, D.B., Mercado, L.M., Sitch, S., Jones, C.D., Gedney, N., Best, M.J., Pryor, M., Rooney, G.G., Essery, R.L.H., Blyth, E., Boucher, O., Harding, R.J., Huntingford, C. and Cox, P.M., 2011. The Joint UK Land Environment Simulator (JULES), model description – Part 2: Carbon fluxes and vegetation dynamics. *Geoscientific Model Development*.

Collatz, G.J., Ball, J.T., Grivet, C. and Berry, J.A., 1991. Physiological and Environmental-Regulation of Stomatal Conductance, Photosynthesis and Transpiration - a Model That Includes a Laminar Boundary-Layer. *Agricultural and Forest Meteorology*, **54**(2–4): 107–136.

Collins, L., Griffioen, P., Newell, G. and Mellor, A., 2018. The utility of Random Forests for wildfire severity mapping. *Remote Sensing of Environment*, **216**(December 2017): 374–384.

Cowan, I.R. and Farquhar, G.D., 1977. Stomatal function in relation to leaf metabolism and environment. *Symposia of the Society for Experimental Biology*, **31**(1973): 471–505. Available at: http://www.ncbi.nlm.nih.gov/pubmed/756635.

Coyle, D.B., Stysley, P.R., Poulios, D., Clarke, G.B. and Kay, R.B., 2015. Laser transmitter development for NASA's Global Ecosystem Dynamics Investigation (GEDI) lidar. pp.961207–961208. Available at: https://doi.org/10.1117/12.2191569.

Cruz, M.G., McCaw, W.L., Anderson, W.R. and Gould, J.S., 2013. Fire behaviour modelling in semi-arid mallee-heath shrublands of southern Australia. *Environmental Modelling and Software*.

Department of Sustainability and Environment, 2012. *2009 Bushfire Recovery Program*. Melbourne, Australia.

Donohue, R.J., Hume, I.H., Roderick, M.L., McVicar, T.R., Beringer, J., Hutley, L.B., Gallant, J.C., Austin, J.M., van Gorsel, E., Cleverly, J.R., Meyer, W.S. and Arndt, S.K., 2014. Evaluation of the remote-sensing-based DIFFUSE model for estimating photosynthesis of vegetation. *Remote Sensing of Environment*, **155**: 349–365. Available at: http://dx.doi.org/10.1016/j.rse.2014.09.007.

Donohue, R.J., Roderick, M.L. and McVicar, T.R., 2007. On the importance of including vegetation dynamics in Budyko's hydrological model. *Hydrology and Earth System Sciences*, **11**(2): 983–995.

Donohue, R.J., Roderick, M.L. and McVicar, T.R., 2008. Deriving consistent long-term

vegetation information from AVHRR reflectance data using a cover-triangle-based framework. *Remote Sensing of Environment*, **112**(6): 2938–2949.

Drusch, M., Del Bello, U., Carlier, S., Colin, O., Fernandez, V., Gascon, F., Hoersch, B., Isola, C., Laberinti, P., Martimort, P., Meygret, A., Spoto, F., Sy, O., Marchese, F. and Bargellini, P., 2012. Sentinel-2: ESA's Optical High-Resolution Mission for GMES Operational Services. *Remote Sensing of Environment*.

Edwards, A.C., Maier, S.W., Hutley, L.B., Williams, R.J. and Russell-Smith, J., 2013. Spectral analysis of fire severity in north Australian tropical savannas. *Remote Sensing of Environment*, **136**: 56–65. Available at: http://dx.doi.org/10.1016/j.rse.2013.04.013.

Ehleringer, J.R. and Field, C.B., 1993. *Scaling Physiological Processes: Leaf to Globe*. [online] *Physiological Ecology: A Series of Monographs, Texts, and Treatises*. Available at: http://dx.doi.org/10.1016/B978-0-12-424210-4.50017-6.

Esplin, B., Gill, M.A. and Enright, N.J., 2003. *Report of the Inquiry into the 2002-2003 Victorian Bushfires*. Melbourne, Australia.

Fensholt, R., Sandholt, I. and Rasmussen, M.S., 2004. Evaluation of MODIS LAI, fAPAR and the relation between fAPAR and NDVI in a semi-arid environment using in situ measurements. *Remote Sensing of Environment*, **91**(3–4): 490–507.

Field, C.B., Randerson, J.T. and Malmström, C.M., 1995. Global net primary production: Combining ecology and remote sensing. *Remote Sensing of Environment*, **51**(1): 74–88.

Fisher, R.A., Muszala, S., Verteinstein, M., Lawrence, P., Xu, C., McDowell, N.G., Knox, R.G., Koven, C., Holm, J., Rogers, B.M., Spessa, A., Lawrence, D. and Bonan, G., 2015. Taking off the training wheels: The properties of a dynamic vegetation model without climate envelopes, CLM4.5(ED). *Geoscientific Model Development*.

Fleck, I., Hogan, K.P., Llorens, L., Abadía, a. and Aranda, X., 1998. Photosynthesis and photoprotection in Quercus ilex resprouts after fire. *Tree physiology*, **18**(8_9): 607–614. Available at: http://www.ncbi.nlm.nih.gov/pubmed/12651349.

Flexas, J., Loreto, F. and Medrano, H., 2011. *Terrestrial photosynthesis in a changing environment. Terrestrial Photosynthesis in a Changing Environment a Molecular, Physiological and Ecological Approach*.

Foster, C.N., Barton, P.S., Robinson, N.M., MacGregor, C.I. and Lindenmayer, D.B., 2017. Effects of a large wildfire on vegetation structure in a variable fire mosaic. *Ecological Applications*.

Gamon, J.A., Field, C.B., Goulden, M.L., Griffin, K.L., Hartley, A.E., Joel, G., Penuelas, J. and Valentini, R., 1995. Relationships Between NDVI , Canopy Structure , and Photosynthesis in Three Californian Vegetation Types Published by : Wiley Stable URL : http://www.jstor.org/stable/1942049 REFERENCES Linked references are available on JSTOR for this article : You may n. *Ecological Applications*, **5**(1): 28–41. Available at: http://www.jstor.org/stable/1942049.

Gharun, M., Possell, M., Vervoort, R.W., Adams, M.A. and Bell, T.L., 2018. Can a growth model be used to describe forest carbon and water balance after fuel reduction burning in temperate forests? *Science of the Total Environment*, **615**: 1000–1009. Available at: https://doi.org/10.1016/j.scitotenv.2017.09.315.

Giglio, L., Schroeder, W. and Justice, C.O., 2016. The collection 6 MODIS active fire detection algorithm and fire products. *Remote Sensing of Environment*.

Goerner, A., Reichstein, M., Tomelleri, E., Hanan, N., Rambal, S., Papale, D., Dragoni, D. and Schmullius, C., 2011. Remote sensing of ecosystem light use efficiency with MODIS-based PRI. *Biogeosciences*, **8**(1): 189–202.

Goulden, M.L., Mcmillan, A.M.S., Winston, G.C., Rocha, A. V, Manies, K.L., Harden, J.W. and Bond-Lamberty, B.P., 2011. Patterns of NPP, GPP, respiration, and NEP during boreal forest succession. *Global Change Biology*, **17**(2): 855–871. Available at: https://www.scopus.com/inward/record.uri?eid=2-s2.0-78650782887&doi=10.1111%2Fj.1365-2486.2010.02274.x&partnerID=40&md5=41dbb1a64689f3c4e9d5daa658d3b77c.

Haverd, V., Raupach, M.R., Briggs, P.R., Canadell., J.G., Davis, S.J., Law, R.M., Meyer, C.P., Peters, G.P., Pickett-Heaps, C. and Sherman, B., 2013. The Australian terrestrial carbon budget. *Biogeosciences*.

Hetherington, S.E., Smillie, R.M. and Davies, W.J., 1998. Photosynthetic activities of vegetative and fruiting tissues of tomato. *Journal of Experimental Botany*, **49**(324): 1173–1181.

Hicke, J.A., Asner, G.P., Kasischke, E.S., French, N.H.F., Randerson, J.T., Collatz, G.J., Stocks, B.J., Tucker, C.J., Los, S.O. and Field, C.B., 2003. Postfire response of North American boreal forest net primary productivity analyzed with satellite observations. *Global Change Biology*, **9**(8): 1145–1157.

Hilker, T., Coops, N.C., Hall, F.G., Nichol, C.J., Lyapustin, A., Black, T.A., Wulder, M.A., Leuning, R., Barr, A., Hollinger, D.Y., Munger, B. and Tucker, C.J., 2011. Inferring terrestrial photosynthetic light use efficiency of temperate ecosystems from space. *Journal of Geophysical Research: Biogeosciences*, **116**(3): 1–11.

Hislop, S., Jones, S., Soto-Berelov, M., Skidmore, A., Haywood, A. and Nguyen, T.H., 2018. Using landsat spectral indices in time-series to assess wildfire disturbance and recovery. *Remote Sensing*, **10**(3): 1–17.

Huang, S., Liu, H., Dahal, D., Jin, S., Welp, L.R., Liu, J. and Liu, S., 2013. Modeling spatially explicit fire impact on gross primary production in interior Alaska using satellite images coupled with eddy covariance. *Remote Sensing of Environment*, **135**: 178–188. Available at: http://dx.doi.org/10.1016/j.rse.2013.04.003.

Huete, A., Didan, K., Miura, H., Rodriguez, E.P., Gao, X. and Ferreira, L.F., 2002. Overview of the radiometric and biopyhsical performance of the MODIS vegetation indices. *Remote Sensing of Environment*, **83**: 195–213. Available at: https://ac-els-cdn-com.sire.ub.edu/S0034425702000962/1-s2.0-S0034425702000962-main.pdf?_tid=420e9dda-1821-11e8-b53d-00000aacb35d&acdnat=1519339356_ef83dc686b96e75a110fbad8d8dc950a.

Hutchinson, M.F., Kesteven, J.L., Xu, T., Stein, J.L., Marang, I.J. and Evans, B.J., 2018. *Daily total solar radiation 2.0, 0.01 degree, Australian Coverage, 1970-present*. Available at: made avaialble by The University of Sydney 07/08/2018.

Ii, H.L. and Carmichael, G.R., 2002. Impacts of biomass burning on tropospheric CO, NOx, and O3. *Fuel and Energy Abstracts*, **43**(x): 142.

Ireland, G. and Petropoulos, G.P., 2015. Exploring the relationships between post-fire vegetation regeneration dynamics, topography and burn severity: A case study from the Montane Cordillera Ecozones of Western Canada. *Applied Geography*, **56**: 232–248. Available at: http://dx.doi.org/10.1016/j.apgeog.2014.11.016.

Jensen, J.R., 2007. Remote Sensing of Vegetation. In: K.C. Clarke, ed., *Remote Sensing of Environment*. New Jersey, USA: Prentice Hall Series in Geographic Information Science, pp.333–377.

Jung, M., Reichstein, M. and Bondeau, A., 2009. Towards global empirical upscaling of FLUXNET eddy covariance observations: Validation of a model tree ensemble approach using a biosphere model. *Biogeosciences*, **6**(10): 2001–2013.

Justice, C.O., Vermote, E.F., Townshend, J.R.G., Defries, R.S., Roy, D.P., Hall, D.K., Salomonson, V. V, Privette, J.L., Riggs, G., Strahler, A.H., Lucht, W., Myneni, R.B., Knyazikhin, Y., Running, S.W., Nemani, R.R., Wan, Z., Huete, A.R., van Leeuwen, W., Wolfe, R.E., Giglio, L., Muller, J.P., Lewis, P. and Barnsley, M., 1998. The Moderate Resolution Imaging Spectroradiometer (MODIS): land remote sensing for global change research. *Geoscience and Remote Sensing, IEEE Transactions on*, **36**(4): 1228–1249. Available at: http://ieeexplore.ieee.org/xpls/abs_all.jsp?arnumber=701075%5Cnpapers2://publication/doi/10.1109/36.701075.

Keeley, J.E., 2009. Fire intensity, fire severity and burn severity: A brief review and suggested usage. *International Journal of Wildland Fire*, **18**(1): 116–126.

Keith, H., Mackey, B., Berry, S., Lindenmayer, D. and Gibbons, P., 2010. Estimating carbon carrying capacity in natural forest ecosystems across heterogeneous landscapes: addressing sources of error. *Global Change Biology*.

Kelliher, F.M., Leuning, R., Raupach, M.R. and Schulze, E.D., 1995. Maximum conductances for evaporation from global vegetation types. *Agricultural and Forest Meteorology*.

Kenny, S.A., Bennett, A.F., Clarke, M.F. and Morgan, J.W., 2018. Time-since-fire and climate interact to affect the structural recovery of an Australian semi-arid plant community. *Austral Ecology*.

Key, C.H. and Benson, N.C., 2006. Landscape assessment: Sampling and analysis methods. *USDA Forest Service General Technical Report RMRS-GTR-164-CD*, (June): 1–55.

Kokaly, R.F., Rockwell, B.W., Haire, S.L. and King, T.V.V., 2007. Characterization of post-fire surface cover, soils, and burn severity at the Cerro Grande Fire, New Mexico, using hyperspectral and multispectral remote sensing. *Remote Sensing of Environment*.

Land Conservation Council, 1987. *Mallee Area Review Descriptive Report*. Melbourne, Australia.

Lauer, M.J. and Boyer, J.S., 1992. Internal CO2 Measured Directly in Leaves : Abscisic Acid and Low Leaf Water Potential Cause Opposing Effects. *Plant Physiology*, **98**(4): 1310–1316. Available at: http://www.plantphysiol.org/cgi/doi/10.1104/pp.98.4.1310.

Leuning, R., Kelliher, F.M., De Pury, D.G.G. and Schulze, E., 1995. Leaf nitrogen, photosynthesis, conductance and transpiration: scaling from leaves to canopies. *Plant, Cell & Environment*, **18**(10): 1183–1200.

Lutes, D.C., Keane, R.E., Caratti, J.F., Key, C.H., Benson, N.C., Sutherland, S. and Gangi, L.J., 2006. *FIREMON: Fire effects monitoring and inventory system. Gen. Tech. Rep. USDA Forest Service RMRS-GTR-164-CD*.

Madani, N., Kimball, J.S., Affleck, D.L.R., Kattge, J., Graham, J., van Bodegom, P.M., Reich, P.B. and Running, S.W., 2014. Improving ecosystem productivity modeling through spatially explicit estimation of optimal light use efficiency. *Journal of Geophysical Research: Biogeosciences*, **119**(i): 1755–1769.

Di Mauro, B., Fava, F., Busetto, L., Crosta, G.F. and Colombo, R., 2014. Post-fire resilience in the Alpine region estimated from MODIS satellite multispectral data. *International Journal of Applied Earth Observation and Geoinformation*, **32**: 163–172. Available at: https://www.sciencedirect.com/science/article/pii/S0303243414000944?via%3Dihub. Online (8

Feb. 2018).

Mercado, L.M., Bellouin, N., Sitch, S., Boucher, O., Huntingford, C., Wild, M. and Cox, P.M., 2009. Impact of changes in diffuse radiation on the global land carbon sink. *Nature*, **458**(7241): 1014–7. Available at: http://www.ncbi.nlm.nih.gov/pubmed/19396143.

Mills, G.A., 2005. On the subsynoptic-scale meteorology of two extreme fire weather days during the Eastern Australian fires of January 2003. **54**(4): 265–290. Available at: https://www.scopus.com/record/display.uri?eid=2-s2.0-33645833191&origin=resultslist&sort=cp-f&src=s&st1=canberra+AND+2003+AND+bushfire&nlo=&nlr=&nls=&sid=90bdf23040e8f2aa2b1b2be2664cefa0&sot=b&sdt=b&sl=45&s=TITLE-ABS-KEY%28canberra+AND+2003+AND+bushfire%29&relpos=0&citeCnt=35&searchTerm=. Online (23 Mar. 2018).

Monteith, J. and Unsworth, M., 2013. *Principles of Environmental Physics: Plants, Animals, and the Atmosphere: Fourth Edition*. *Principles of Environmental Physics: Plants, Animals, and the Atmosphere: Fourth Edition*.

Monteith, J.L., 1965. Evaporation and environment. *Symposia of the Society for Experimental Biology*.

Monteith, J.L., 1972. Solar Radiation and Productivity in Tropical Ecosystems. *Journal of Applied Ecology*, **9**(3): 747–766. Available at: http://www.jstor.org/stable/2401901.

Murphy, B.P., Bradstock, R.A., Boer, M.M., Carter, J., Cary, G.J., Cochrane, M.A., Fensham, R.J., Russell-Smith, J., Williamson, G.J. and Bowman, D.M.J.S., 2013. Fire regimes of Australia: A pyrogeographic model system. *Journal of Biogeography*, **40**(6): 1048–1058.

Myneni, R.B., Los, S.O. and Asrar, G., 1995. Potential gross primary productivity of terrestrial vegetation from 1982–1990. *Geophysical Research Letters*, **22**(19): 2617–2620.

National Parks Service and Department of Conservation and Natural Resources, 1994. Big Desert Wilderness Park Management Plan. (July).

Nemani, R.R. and Running, S.W., 1989. Testing a theoretical climate-soil-leaf area hydrologic equilibrium of forests using satellite data and ecosystem simulation. *Agricultural and Forest Meteorology*, **44**(3–4): 245–260.

Nicolle, D., 2006. A classification and census of regenerative strategies in the eucalypts (Angophora, Corymbia and Eucalyptus - Myrtaceae), with special reference to the obligate seeders. *Australian Journal of Botany*, **54**(4): 391–407.

Nolan, R.H., Lane, P.N.J., Benyon, R.G., Bradstock, R.A. and Mitchell, P.J., 2015. Trends in evapotranspiration and streamflow following wildfire in resprouting eucalypt forests. *Journal of Hydrology*, **524**(January): 614–624.

NVIS Technical Working Group, 2017. *Australian Vegetation Attribute Manual: National Vegetation Information System*. Canberra: Department of Environment and Energy.

Odum, E.P., 2014. The strategy of Ecosystem development. In: *The Ecological Design and Planning Reader*. pp.203–216. Available at: http://link.springer.com/10.5822/978-1-61091-491-8_20.

Palace, M.W., Sullivan, F.B., Ducey, M.J., Treuhaft, R.N., Herrick, C., Shimbo, J.Z. and Mota-E-Silva, J., 2015. Estimating forest structure in a tropical forest using field measurements, a synthetic model and discrete return lidar data. *Remote Sensing of Environment*.

Pan, Y., Chen, J.M., Birdsey, R., McCullough, K., He, L. and Deng, F., 2011. Age structure and disturbance legacy of North American forests. *Biogeosciences*.

Park, S. Bin, Knohl, A., Lucas-Moffat, A.M., Migliavacca, M., Gerbig, C., Vesala, T., Peltola, O., Mammarella, I., Kolle, O., Lavrič, J.V., Prokushkin, A. and Heimann, M., 2018. Strong radiative effect induced by clouds and smoke on forest net ecosystem productivity in central Siberia. *Agricultural and Forest Meteorology*.

Parks, S.A., Dillon, G.K. and Miller, C., 2014. A new metric for quantifying burn severity: The relativized burn ratio. *Remote Sensing*, **6**(3): 1827–1844.

Pausas, J.G. and Keeley, J.E., 2014. Evolutionary ecology of resprouting and seeding in fire-prone ecosystems. *New Phytologist*, **204**(1): 55–65.

Polglase, P.J. and Attiwill, P.M., 1992. Nitrogen and phosphorus cycling in relation to stand age of Ecucalyptus regnans F. Muell - I. Return from plant to soil in litterfall. *Plant and Soil*.

Polychronaki, A., Gitas, I.Z. and Minchella, A., 2014. Monitoring post-fire vegetation recovery in the Mediterranean using SPOT and ERS imagery. *International Journal of Wildland Fire*, **23**(5): 631–642.

Potter, C.S., Randerson, J.T., Field, C.B., Matson, P.A., Vitousek, P.M., Mooney, H.A. and Klooster, S.A., 1993. Terrestrial ecosystem production: A process model based on global satellite and surface data. *Global Biogeochemical Cycles*.

De Pury, D.G.G. and Farquhar, G.D., 1997. Simple scaling of photosynthesis from leaves to canopies without the errors of big-leaf models. *Plant, Cell and Environment*, **20**(5): 537–557. Available at: http://doi.wiley.com/10.1111/j.1365-3040.1997.00094.x.

Rocha, A. V. and Shaver, G.R., 2011. Burn severity influences postfire CO 2 exchange in arctic tundra. *Ecological Applications*, **21**(2): 477–489. Available at: http://www.scopus.com/inward/record.url?eid=2-s2.0-79955542336&partnerID=tZOtx3y1.

Roderick, M.L., Farquhar, G.D., Berry, S.L. and Noble, I.R., 2001. On the direct effect of clouds and atmospheric particles on the productivity and structure of vegetation. *Oecologia*, **129**(1): 21–30.

Rogers, A., Medlyn, B.E., Dukes, J.S., Bonan, G., von Caemmerer, S., Dietze, M.C., Kattge, J., Leakey, A.D.B., Mercado, L.M., Niinemets, ï¿½lo, Prentice, I.C., Serbin, S.P., Sitch, S., Way, D.A. and Zaehle, S., 2017. A roadmap for improving the representation of photosynthesis in Earth system models. *New Phytologist*, **213**(1): 22–42.

Roxburgh, S.H., Barrett, D.J., Berry, S.L., Cartel, J.O., Davies, I.D., Gifford, R.M., Kirschbaum, M.U.F., McBeth, B.P., Noble, I.R., Parton, W.G., Raupach, M.R. and Roderick, M.L., 2004. A critical overview of model estimates of net primary productivity for the Australian continent. *Functional Plant Biology*, **31**(11): 1043–1059.

Ruiz, J., Fandiño, M.C.M.C. and Chazdon, R.L.R.L., 2005. Vegetation Structure, Composition, and Species Richness Across a 56-year Chronosequence of Dry Tropical Forest on Providencia Island, Colombia. *Biotropica*.

Running, S.W., Glassy, J. and Thornton, P.E., 1999. *MODIS daily photosynthesis (PSN) and annual net primary production (NPP) product (MOD17) Algorithm Theoretical Basis Document*. *SCF At-Launch Algorithm ATBD Doc*.

Running, S.W., Nemani, R.R., Heinsch, F.A., Zhao, M., Reeves, M. and Hashimoto, H., 2004. A Continuous Satellite-Derived Measure of Global Terrestrial Primary Production. *BioScience*, **54**(6): 547. Available at: https://academic.oup.com/bioscience/article/54/6/547-

560/294347.

Russel, G., Marshall, B. and Jarvis, P.G., 1989. Plant canopies: their growth, form and function. 1–178.

SAS Institute Inc., 2007. *JMP®*.

Schaaf, C. and Wang, Z., 2015. *MCD43A4 MODIS/Terra+Aqua BRDF/Albedo Nadir BRDF Adjusted Ref Daily L3 Global - 500m V006*. Available at: https://doi.org/10.5067/MODIS/MCD43A4.006.

Šesták, Z. and Šiffel, P., 1997. Leaf-age related differences in chlorophyll fluorescence. *Photosynthetica*, **33**(3–4): 347–369. Available at: http://www.scopus.com/scopus/inward/record.url?eid=2-s2.0-0000440777&partnerID=40&rel=R6.5.0.

Sims, D.A. and Gamon, J.A., 2002. Relationships between leaf pigment content and spectral reflectance across a wide range of species, leaf structures and developmental stages. *Remote Sensing of Environment*, **81**(2–3): 337–354.

Tempfli, K., Kerle, N., Huuneman, G.C. and Jansen, L.L.F., 2001. *Principles of Remote Remote Sensing - An introductory text book*.

Thomas, V., Gellie, N. and Harrison, T., 2000. Forest ecosystem classification and mapping for the Southern CRA region, Volume II Appendices. A report undertaken for the NSW CRA/RFA Steering Committee. **II**(March).

Thonicke, K., Spessa, A., Prentice, I.C., Harrison, S.P., Dong, L. and Carmona-Moreno, C., 2010. The influence of vegetation, fire spread and fire behaviour on biomass burning and trace gas emissions: Results from a process-based model. *Biogeosciences*, **7**(6): 1991–2011.

Tucker, C.J., 1979. Red and photographic infrared linear combinations for monitoring vegetation. *Remote Sensing of Environment*, **8**(2): 127–150.

Tucker, C.J. and Sellers, P.J., 1986. Satellite remote sensing of primary production. *International Journal of Remote Sensing*, **7**(11): 1395–1416.

Turner, D.P., Ritts, W.D., Styles, J.M., Yang, Z., Cohen, W.B., Law, B.E. and Thornton, P.E., 2006a. A diagnostic carbon flux model to monitor the effects of disturbance and interannual variation in climate on regional NEP. *Tellus, Series B: Chemical and Physical Meteorology*, **58**(5): 476–490.

Turner, D.P., Ritts, W.D., Styles, J.M., Yang, Z., Cohen, W.B., Law, B.E. and Thornton, P.E., 2006b. A diagnostic carbon flux model to monitor the effects of disturbance and interannual variation in climate on regional NEP. *Tellus, Series B: Chemical and Physical Meteorology*, **58**(5): 476–490.

Tuzet, A., Perrier, A. and Leuning, R., 2003. A coupled model of stomatal conductance , photosynthesis. *Plant, Cell and Environment*, **26**: 1097–1116.

Verma, M., Schimel, D., Evans, B., Frankenberg, C., Beringer, J., Drewry, D.T., Magney, T., Marang, I., Hutley, L., Moore, C. and Eldering, A., 2017. Effect of environmental conditions on the relationship between solar-induced fluorescence and gross primary productivity at an OzFlux grassland site. *Journal of Geophysical Research: Biogeosciences*, **122**(3): 716–733. Available at: http://doi.wiley.com/10.1002/2016JG003580.

Vivian, L.M., Cary, G.J., Bradstock, R.A. and Gill, A.M., 2008. Influence of fire severity on the regeneration, recruitment and distribution of eucalypts in the Cotter River Catchment,

Australian Capital Territory. *Austral Ecology*.

Walz, Y., Maier, S.W., Dech, S.W., Conrad, C. and Colditz, R.R., 2007. Classification of burn severity using Moderate Resolution Imaging Spectroradiometer (MODIS): A case study in the jarrah-marri forest of southwest Western Australia. *Journal of Geophysical Research: Biogeosciences*, **112**(2): 1–14.

Wu, X., Ju, W., Zhou, Y., He, M., Law, B.E., Black, T.A., Margolis, H.A., Cescatti, A., Gu, L., Montagnani, L., Noormets, A., Griffis, T.J., Pilegaard, K., Varlagin, A., Valentini, R., Blanken, P.D., Wang, S., Wang, H., Han, S., Yan, J., Li, Y., Zhou, B. and Liu, Y., 2015. Performance of linear and nonlinear two-leaf light use efficiency models at different temporal scales. *Remote Sensing*, **7**(3): 2238–2278.

Yan, H., Wang, S.Q., Yu, K.L., Wang, B., Yu, Q., Bohrer, G., Billesbach, D., Bracho, R., Rahman, F. and Shugart, H.H., 2017. A Novel Diffuse Fraction-Based Two-Leaf Light Use Efficiency Model: An Application Quantifying Photosynthetic Seasonality across 20 AmeriFlux Flux Tower Sites. *Journal of Advances in Modeling Earth Systems*.

Yebra, M., 2018. *Fire history vector files for every state and territory authority in Australia.* Available at: Made available by the researcher, not for publication or public dissemination.

Yebra, M., Dennison, P.E., Chuvieco, E., Riaño, D., Zylstra, P., Hunt, E.R., Danson, F.M., Qi, Y. and Jurdao, S., 2013a. A global review of remote sensing of live fuel moisture content for fire danger assessment: Moving towards operational products. *Remote Sensing of Environment*, **136**: 455–468.

Yebra, M., Van Dijk, A., Leuning, R., Huete, A. and Guerschman, J.P., 2013b. Evaluation of optical remote sensing to estimate actual evapotranspiration and canopy conductance. *Remote Sensing of Environment*, **129**: 250–261. Available at: http://dx.doi.org/10.1016/j.rse.2012.11.004.

Yebra, M., Van Dijk, A.I.J.M., Leuning, R. and Guerschman, J.P., 2015. Global vegetation gross primary production estimation using satellite-derived light-use efficiency and canopy conductancejarvis. *Remote Sensing of Environment*, **163**: 206–216. Available at: http://dx.doi.org/10.1016/j.rse.2015.03.016.

Zhang, Q., M. Chen, J., Ju, W., Wang, H., Qiu, F., Yang, F., Fan, W., Huang, Q., Wang, Y. ping, Feng, Y., Wang, X. and Zhang, F., 2017. Improving the ability of the photochemical reflectance index to track canopy light use efficiency through differentiating sunlit and shaded leaves. *Remote Sensing of Environment*, **194**: 1–15. Available at: http://dx.doi.org/10.1016/j.rse.2017.03.012.

Zhao, M., Heinsch, F.A., Nemani, R.R. and Running, S.W., 2005. Improvements of the MODIS terrestrial gross and net primary production global data set. *Remote Sensing of Environment*, **95**(2): 164–176.

Zhou, T., Shi, P., Jia, G., Dai, Y., Zhao, X., Shangguan, W., Du, L., Wu, H. and Luo, Y., 2015. Age-dependent forest carbon sink: Estimation via inverse modeling. *Journal of Geophysical Research: Biogeosciences*, **120**(12): 2473–2492.

Appendix 1 – Fire scar mean GPP time series with radiation and conductance components separated.

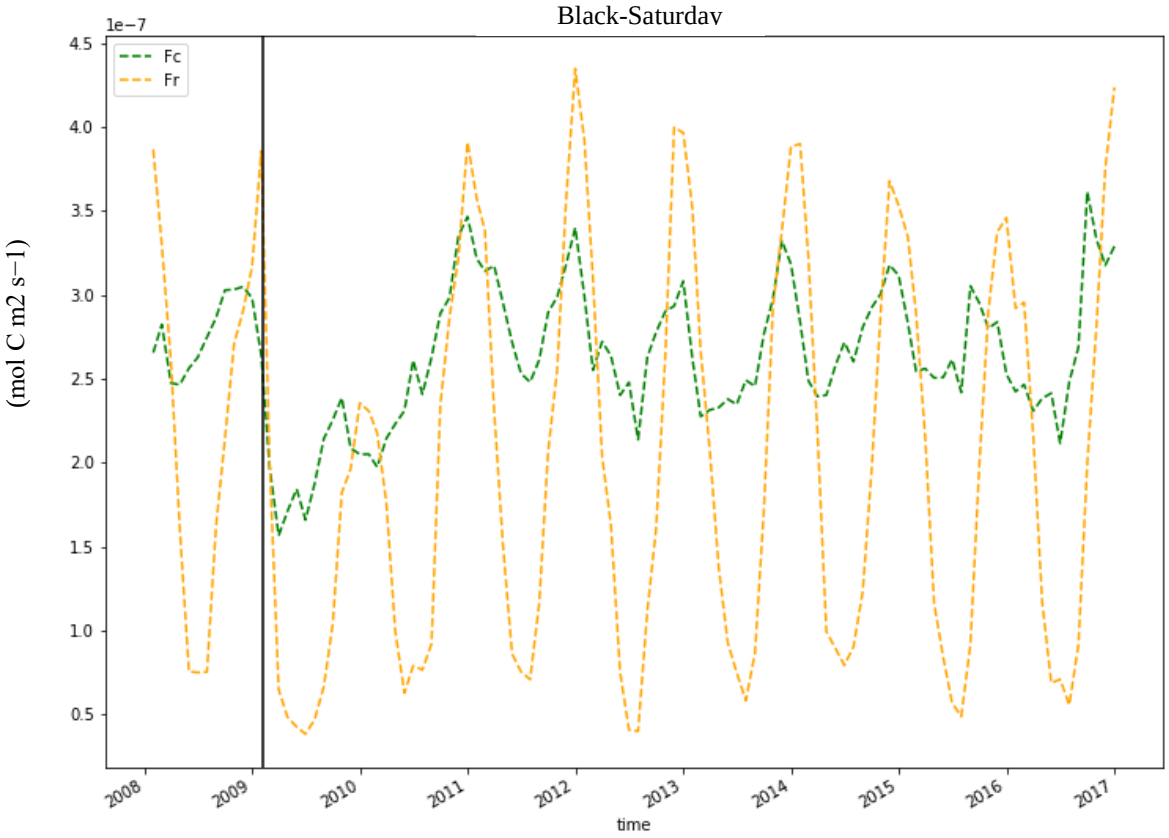

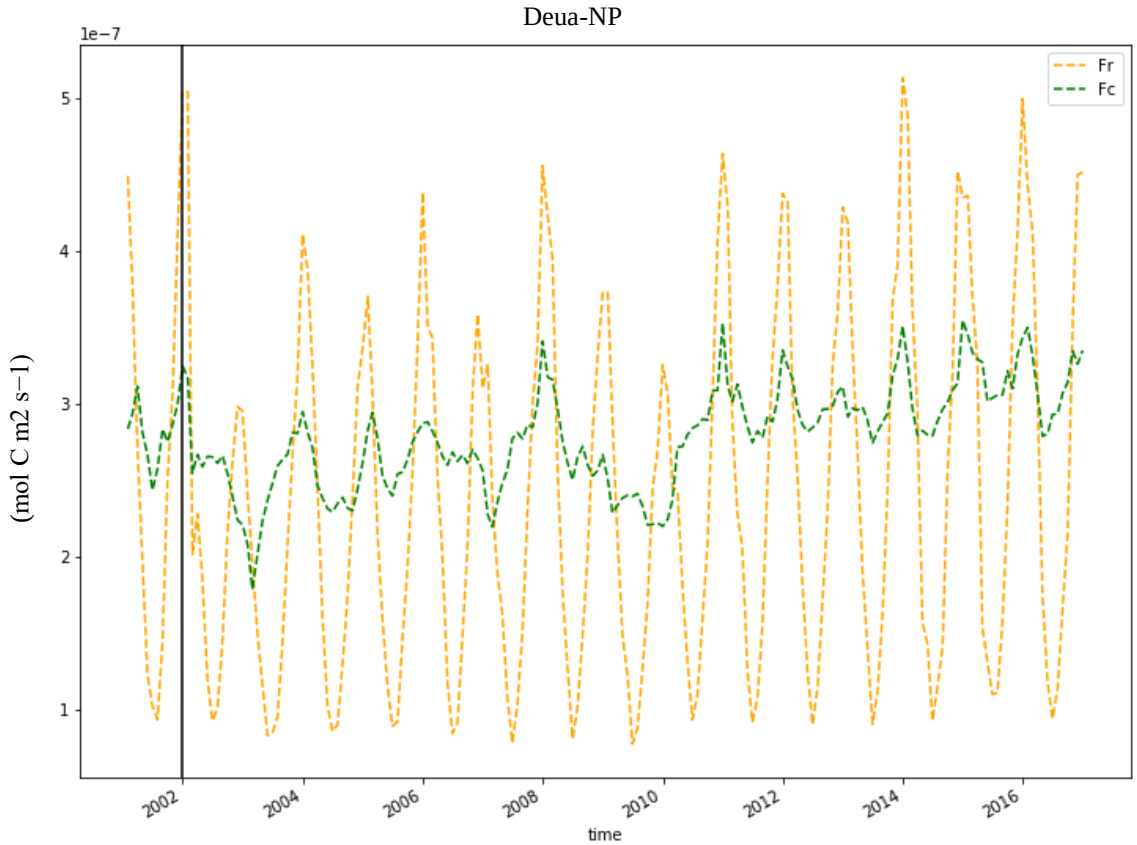

Brindabella

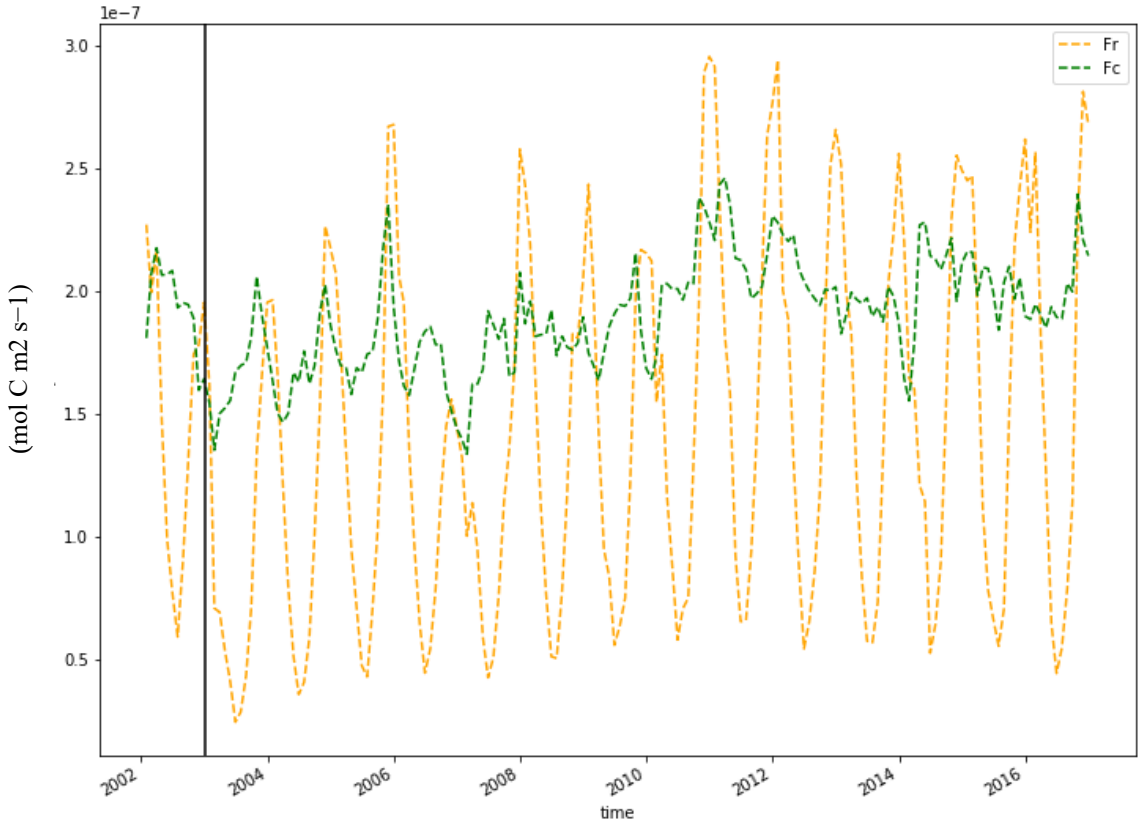

Big-Desert

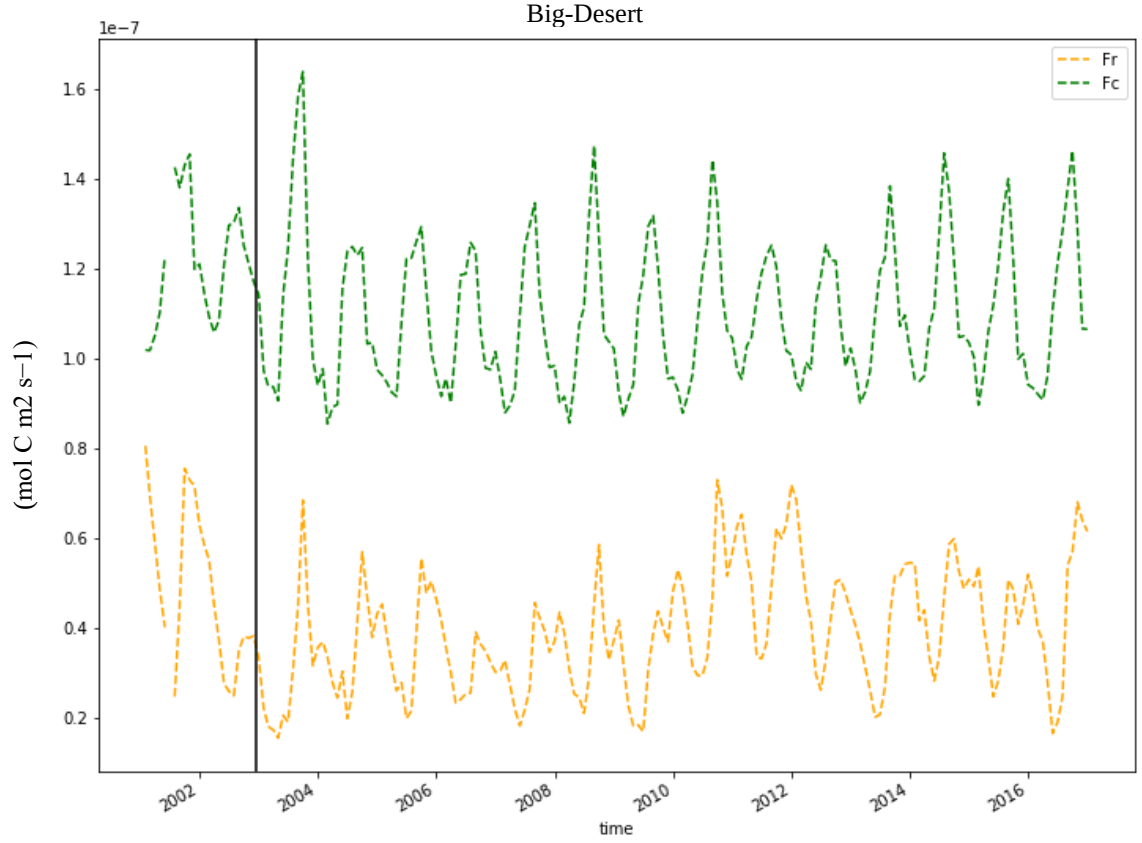

Appendix 2 – GPP model code (python)

```
# coding: utf-8

"""
Process to compute Gross Primary Production (Yebra et al., 2015)
over region of interest.
Takes satellite reflectance and metereological data.

Credit to Zac Hatfield-Dodds (https://github.com/Zac-HD) for basic
MODIS manipulation and zooming functions.
"""
import xarray as xr
import numpy as np
import matplotlib.pyplot as plt
import scipy.stats as sci
import gdal
from copy import deepcopy
from scipy.ndimage import zoom as ndzoom
import pandas as pd
import glob
import datetime
import typing as t
from pathlib import Path
import re
import subprocess as sp
import collections
import json
from osgeo import gdal, gdalconst, ogr, gdal_array, osr
import sys, os,  math, tempfile


"""
General purpose functions for loading MODIS data.
This script is used for loading reflectance and restoring physical
coordinates
to an array for a given tile.
"""

xr_data_type = t.Union[xr.Dataset, xr.DataArray]

modis_band_map = {
    'Nadir_Reflectance_Band1': 'red_630_690',
    'Nadir_Reflectance_Band2': 'nir1_780_900',
    'Nadir_Reflectance_Band3': 'blue_450_520',
    'Nadir_Reflectance_Band4': 'green_530_610',
    'Nadir_Reflectance_Band5': 'nir2_1230_1250',
    'Nadir_Reflectance_Band6': 'swir1_1550_1750',
    'Nadir_Reflectance_Band7': 'swir2_2090_2350',
}


def add_tile_coords(tile: str, dataset: xr_data_type) ->
xr_data_type:
    """Restore physical coordinates to dataset."""
    scale = 1111950.5196669996
    regex = re.compile('h\d+v\d+')
    matches = regex.findall(tile)
    extract = re.compile('\d+')
```

```
    h, v = extract.findall(matches[0])
    h = int(h)
    v = int(v)
    x_start = scale * (h - 18)
    x_end = scale * (h - 17)
    y_start = -scale * (v - 9)
    y_end = -scale * (v - 8)
    dataset['x'] = xr.IndexVariable('x', np.linspace(x_start,
x_end, 2400))
    dataset['y'] = xr.IndexVariable('y', np.linspace(y_start,
y_end, 2400))
    return dataset


def difference_index(a: xr.DataArray, b: xr.DataArray) ->
xr.DataArray:
    """Get difference index between bands used in NDVI, NDII,
etc."""
    return ((a - b) / (a + b)).astype('float32')

def enhanced_index(a: xr.DataArray, b: xr.DataArray,
c:xr.DataArray) -> xr.DataArray:
    """Get enhanced difference index"""
    return (2.5 * ((a - b) / (a + 6 * b - 7.5 * c +
1))).astype('float32')

def moisture_index(a: xr.DataArray, b: xr.DataArray) ->
xr.DataArray: # takes gvmi and evi as parameters
            """Get residual moisture index"""
            krmi = 0.775
            crmi = -0.0757
            return ((a - (krmi * b +
crmi)).clip(min=0,max=1)).astype('float32')

def rescale(a: xr.DataArray, x_min: int, x_max: int) ->
xr.DataArray:
    """Rescale any array between max and min values"""
    return ((a - x_min) / (x_max - x_min)).astype('float32')

def crop_factor(l: xr.DataArray, m: xr.DataArray) -> xr.DataArray:
# takes evir and rmi as parameters
    kcmax, a, alpha, b, beta = 0.68, 14.12, 2.482, 7.991, 0.890
    return (kcmax * (1-xr.ufuncs.exp(-a*(l**alpha)-
b*(m**beta)))).astype('float32')

reflectance_file_cache = []  # type: t.List[str]


def get_reflectance(yr: int, tile: str) -> xr.Dataset:
    """Load reflectance data for one tile-year."""
    #global reflectance_file_cache
    #if not reflectance_file_cache:
    reflectance_file_cache[:] = sorted(glob.glob(
            '/g/data/u39/public/data/modis/lpdaac-tiles-
c6/MCD43A4.006/' +
            '{yr}.??.??/MCD43A4.A{yr}???.h??v??.006.*.hdf'
            .format(yr=yr)
        ))
    files = [f for f in reflectance_file_cache if tile in
Path(f).name]
```

```
    pattern =
re.compile(r'MCD43A4.A\d{4}(?P<day>\d{3}).h\d\dv\d\d.006.\d+'
                           '.hdf')
    dates, parts = [], []
    for f in files:
        try:
            parts.append(xr.open_dataset(f, chunks=2400))
            day, = pattern.match(Path(f).name).groups()
            dates.append(datetime.date(int(yr), 1, 1) +
                         datetime.timedelta(days=int(day) - 1))
        except Exception:
            print('Could not read from ' + f)

    date_series = pd.to_datetime(dates)
    date_series.name = 'time'

    ds = xr.concat(parts, date_series)
    out = xr.Dataset()
    for i in map(str, range(1, 8)):
        key = 'Nadir_Reflectance_Band' + i
        data_ok = ds['BRDF_Albedo_Band_Mandatory_Quality_Band' + i]
== 0
        out[modis_band_map[key]] =
ds[key].where(data_ok).astype('f4')
    out['ndvi_ok_mask'] = 0.15 < difference_index(out.nir1_780_900,
out.red_630_690)
    out['ndii'] = difference_index(out.nir1_780_900,
out.swir1_1550_1750)
    out['ndvi'] = difference_index(out.nir1_780_900,
out.red_630_690)
    out['evi'] = enhanced_index(out.nir1_780_900, out.red_630_690,
out.blue_450_520)
    out['gvmi'] = difference_index((out.nir1_780_900 +
0.1),(out.nir1_780_900 + 0.02))
    out['evir'] = (rescale(out.evi,0,0.9).clip(min=0, max=1))#
evimin = 0, evimax = 0.9
    out['rmi'] = moisture_index(out.gvmi,out.evi) # takes gvmi and
evi as parameters
    out['kc'] = crop_factor(out.evir,out.rmi) # takes evir and rmi
as parameters

    xy_names = {'YDim:MOD_Grid_BRDF': 'y', 'XDim:MOD_Grid_BRDF':
'x'}

    try:
        out.rename(xy_names, inplace=True)
    except ValueError:
        pass
    out.time.encoding.update(dict(
        units='days since 1900-01-01', calendar='gregorian',
dtype='i4'))
    return add_tile_coords(tile, out)


def call_gdalbash():
    for arr in list(glob.glob(path+'*.nc')):
        commands ='gdalwarp -s_srs "+proj=sinu +lon_0=0 +x_0=0
+y_0=0 +a=6371007.181 +b=6371007.181 +units=m +no_defs" -t_srs
"EPSG:4326" -tr 0.005 0.005 -overwrite '+arr+' '+arr+'_latlon.tif'
        sp.check_call('bash && module load gdal && '+commands,
shell=True, executable='/bin/bash')
```

```
    return


def subset_build_tif(time_stamps):
    # open whole tile tif with rasterio, rename dimensions, add
time and drop band coords/dims
    ## write this loop for each array of input? dont want to but
will have to open each array to memory? as dask?

    for d in list(glob.glob(path+'*_latlon.tif')):
        tif_file = xr.open_rasterio(d, chunks = dict(band=46,
x=800, y=800))
        names = ['rmi','ndvi','evi','gvmi','kc']
        for i in names:
            if i in d:
                variable = str(i)
        tif_data =
tif_file.to_dataset(name=variable).rename({'y':'latitude',
'x':'longitude'})
        tif_data.coords['time'] = ('band',time_stamps)
        input_var = tif_data.swap_dims({'band':
'time'}).drop('band')
        input_sub =
input_var.sel(longitude=slice(min_lon,max_lon),latitude=slice(max_l
at,min_lat))
        input_sub.to_netcdf(path+'_'+variable+'_prep.nc',mode='w')
    # add command to catch outputs of for loop, and then return
dataset, passing to gc and fr functions in multi_call
    return


def zoom_data(blocky):
    # array in the desired 0.005 res in lat/lon (from VI
preparation)
    details = xr.open_dataarray(path+'_evi_prep.nc').fillna(0)
    # use deepcopy to duplicate LUE as new zooming dataset, add in
radiation metadata
    # use radiation timesteps in time dimension
    smooth = deepcopy(details)
    smooth.attrs = blocky.attrs
    smooth.name = blocky.name
    smooth['time'] = blocky.time

    # select cubic spline, order 3 in zoom function
    SPLINE_ORDER = 3  # Try some other values 0 to 5 for
SPLINE_ORDER to see what happens
    # zoom is ratio between fine and course datasets of length of
cells over lat and lon
    ZOOM_FACTOR = (len(details.latitude) / len(blocky.latitude),
                   len(details.longitude) / len(blocky.longitude))

    # It's also possible to zoom a 3D array by setting a factor of
1 for the time
    # dimension, but this way we preserve the timesteps correctly.
    for timestamp in smooth.time:
        # Start by selecting the timestamp
        data = blocky.sel(time=timestamp)
        # Then zoom to the desired scale, filling nodata values
with zero so we can zoom
        output = ndzoom(np.nan_to_num(data), zoom=ZOOM_FACTOR,
order=SPLINE_ORDER)
```

```
        # Assign output to the contents of the fine_moisture array
        fine = smooth.sel(time=timestamp)
        fine[:] = output

        # Make sure the minimum is zero, so it remains physically
plausible
        fine.values[fine.values < 0] = 0
        # Last, we'll copy both sets of NaN values so that we don't
cause spurious correlations
        # Try commenting each of these out to see how the map
changes!
#         fine.values[np.isnan(details.sel(time=timestamp).values)]
= np.nan  # from the high-res data
        fine.values[ndzoom(np.isnan(data), zoom=ZOOM_FACTOR,
order=0)] = np.nan  # from low-res, with nearest (blocky) zooming
    return smooth


def bash_rm_tif():
    sp.check_call(['rm '+path+'*tif'], shell=True,
executable='/bin/bash')# could add sp.wait() if subsequent
functions cant find produced files
    return


def calculate_gcVI(period,site):
    # needs datasets as wgs84
    # call dataset in arg or in function?
    # need to combine arrays of tif in subset_tif()
    if os.path.isfile(path+'*_vigc.nc'):
        print('gc for each VI already stored in NETCDF per year')
    else:
        # open dataset from subset_build_tif()
        ds = xr.open_mfdataset(path+'*_prep.nc') # add chunks
        period = int(ds['time.year'][0])
        # compute gc for each VI
        gcndvi = (0.0020 * xr.ufuncs.exp(4.11 * (ds.ndvi -
0.4))).rename('ndviGC')
        gcevi = (0.0025 * xr.ufuncs.exp(3.15 * (ds.evi -
0.1))).rename('eviGC')
        gckc = (0.0003 * xr.ufuncs.exp(5.14* (ds.kc -
0))).rename('kcGC')

        # merge all data to gc file for that year
        vigc = xr.merge((gcndvi, gcevi, gckc))
        vigc.to_netcdf(path+'_vigc.nc', mode='w')
    return calculate_gcVPD(vigc,period,site)


def subset_latlon(dataset,date):
    #subset nc file of radiation data
    ds = xr.open_mfdataset(dataset, chunks=dict(lat=115, lon=176,
time=73))
    layout = ds.rename({'lat':'latitude', 'lon':'longitude'})
.sel(time=(slice(str(date),str(date),4)))
    var = next(iter(layout.data_vars.keys()))
    sub =
layout.sel(longitude=slice(min_lon,max_lon),latitude=slice(max_lat,
min_lat))
    out = sub[str(var)]
    return out
```

```
def fract_years(data: xr.DataArray): # does it need to be array?
    time = data.time.values
    df = pd.DataFrame({'dates':time})
    df['day'] = df['dates'].dt.dayofyear * (1/365)
    fyear = df.to_xarray().day
    return xr.concat(data, fyear).swap_dims({'index':
'time'}).drop('index')


def shape_mask(template,site):
    shapefile =
glob.glob('/g/data/xc0/user/IvanK/thesis_data/fire_area/'+site+'.sh
p')[0]
    xmin,ymin,xmax,ymax=min_lon,min_lat,max_lon,max_lat
    nrows,ncols=template.isel(time=0).shape
    maskvalue = 1

    xres=(xmax-xmin)/float(ncols)
    yres=(ymax-ymin)/float(nrows)
    geotransform=(xmin,xres,0,ymax,0, -yres)

    src_ds = ogr.Open(shapefile)
    src_lyr=src_ds.GetLayer()

    dst_ds = gdal.GetDriverByName('MEM').Create('', ncols, nrows, 1
,gdal.GDT_Byte)
    dst_rb = dst_ds.GetRasterBand(1)
    dst_rb.Fill(0) #initialise raster with zeros
    dst_rb.SetNoDataValue(0)
    dst_ds.SetGeoTransform(geotransform)

    err = gdal.RasterizeLayer(dst_ds, [maskvalue], src_lyr)
    dst_ds.FlushCache()

    mask_arr=dst_ds.GetRasterBand(1).ReadAsArray()
    return xr.DataArray(mask_arr,
coords=(template.latitude.values,template.longitude.values),
dims=('latitude','longitude'))


def calculate_gcVPD(period,site):
    D50 = 700
    C1 = 1.94
    if os.path.isfile(path+'*_gc+vpd.nc'):
        print('gc and VPD adjusted gc already stored in NETCDF per
year')
    else:
        # calculate canopy conductanc as average of VI gc
        ds = xr.open_dataset(path+'_vigc.nc'), chunks =
dict(time=46, latitude=30, longitude=30)
        gc = ((gc_from_VIs.ndviGC + gc_from_VIs.eviGC +
gc_from_VIs.kcGC) / 3).rename('GC') # m s-1

        # calculate vdp from tmin, tmax, vp
        # temps converted to K from oC
        tmin =
zoom_data((subset_latlon((glob.glob('/g/data/xc0/user/IvanK/thesis_
data/CLIM/ANUClimate_v2-0_tmin_'+site+'_*.nc')[0]),period)))
```

```
        tmax =
zoom_data((subset_latlon((glob.glob('/g/data/xc0/user/IvanK/thesis_
data/CLIM/ANUClimate_v2-0_tmax_'+site+'_*.nc')[0]),period)))
        e =
zoom_data((subset_latlon((glob.glob('/g/data/xc0/user/IvanK/thesis_
data/CLIM/ANUClimate_v2-0_vp_'+site+'_*.nc')[0]),period)))

    # convert to Pa from hPa
        e = e / 100
        tmin = tmin + 237.15
        tmax = tmax + 237.15

        ta = tmin + (0.75 * (tmax - tmin))
        esat = 610.8 * xr.ufuncs.exp((17.27 * ta)/ (ta + 237.3))
        VPD = (esat - e)

        fD = 1/(1+(VPD/D50))

        gc_vpd = (fD * gc * C1).transpose('time', 'latitude',
'longitude').rename('GCvpd')

        vpdgc = xr.merge((gc, gc_vpd))
        vpdgc.to_netcdf(path+'_gc+vpd.nc', mode='w')
    return canopy_productivity(vpdgc)


# Converts canopy conductance to GPP using a coefficient and
atmospheric concentration of CO2 based on year
def canopy_productivity(final_gc):
    Ro = 0.76 # Ro = Ci / Ca # calculated from fitting Fc below to
validation flux towers globally, could re fit
             # to sites of interest
    Cg = 26
    # call the year of gc data
    fracyear = fract_years(final_gc.GCvpd).day #day of year
(fractional year) of each array of conductance
    Ca = (1.206e-8 * fracyear**2 - 4.641e-5 * fracyear +
0.045).rename('Ca')
        # converts from mm s-1, H20 conductance to umol C m-2 s-1,
CO2 conductance
        # coeficient 41.6 monm-3 follows from the ideal gas law for
standard air pressure an 25C temperature.
        # 1.6 accounts for the greater diffusivity of CO2 compared
to water
    calc = (41.6 / 1.6) * final_gc * (1-Ro) * Ca *
(Daylight(day_years(final_gc.GCvpd)))
    calc.to_netcdf(path+'_GPP_kc_gc.nc', mode='w')
    return calc.rename({'GC': 'Fc_gc', 'GCvpd':
'Fc_gcvpd'}).Fc_gcvpd.drop('day')

###
### start of GPP radiation component
###


# function to compute photosynthetically active radiation (PAR)
from total surface radiation (ANUClimate v2)
def radiation_productivity(period,site):
    surad =
zoom_data((subset_latlon((glob.glob('/g/data/xc0/user/IvanK/thesis_
data/CLIM/ANUClimate_v2-0_srad_'+site+'_*.nc')[0]),period)))
```

```
    # # convert units and for daylight hours
    radiation = (surad * 0.45)
    # 0.45  - percentage of surface radiation that is PAR (based on
Monteith and Unsworth 2013)
    # 4.4 umol photons assumed to equal 1 J PAR
    PAR = radiation * 4.4

    ds = LUE_inputs()
    fr = ds.lue * ds.fpar * PAR * (Daylight(day_years(ds.lue)))
    fr.to_netcdf(path+'_GPP_loc_fr.nc', mode='w')
    return fr.rename('Fr')

def day_years(data: xr.DataArray):
    time = data.time.values
    df = pd.DataFrame({'dates':time})
    df['day'] = df['dates'].dt.dayofyear
    fyear = df.to_xarray().day
    return xr.concat(data, fyear).swap_dims({'index':
'time'}).drop('index')


def Daylight(data): # takes latitudes of array and day of year
(from day_years()) and returns fraction of day with sun for each
cell
    P = xr.ufuncs.arcsin(0.39795 * xr.ufuncs.cos(0.2163108 + 2 *
xr.ufuncs.arctan(0.9671396 * xr.ufuncs.tan(.00860 * (data.day -
186)))))
    pi = np.pi
    lightamounthour = 24 - (24 / pi) *
xr.ufuncs.arccos((xr.ufuncs.sin((0.8333 * pi / 180) +
xr.ufuncs.sin(data.latitude * pi / 180) * xr.ufuncs.sin(P)) /
(xr.ufuncs.cos(data.latitude * pi / 180) * xr.ufuncs.cos(P))))
    fday = lightamounthour * (1/24)
    fday.reset_index(['latitude', 'day'], drop=True, inplace =
True)
    return fday


# function to compute light use productivity efficiency (LUE) from
scaled enhanced
# vegetation index, and productive area (fPAR) from scaled
normalised vegetation index
def LUE_inputs():
    # open dataset of prepared ndvi and evi
    ds = xr.open_mfdataset(path+'*vi_prep.nc',
chunks=dict(latitude=30, longitude=30, time=46))
    evimin = 0.05
    evimax = 0.9
    LUEmax = 0.045 #maximum light use effeciency mol mol-1 (from
EVI scaled)
    R0 = 0.76 #mol mol-1 achieved minimum ratio of internal to
external CO2 concentration

    fPARmax = 0.95
    Fx= 0.9 #maximum fPAR
    Fn= 0.1 #minumum fPAR
    Vx= 0.67 #maximum NDVI 0.85 For Australia 0.67
    Vn= 0.09 #minimum NDVI New global 0.15 For Australia 0.09
```

```
    evir = ((ds.evi - evimin) / (evimax - evimin)).clip(min=0.05,
max=0.9)
    LUE = ((LUEmax * 1e-6) * evir).rename('lue')
    NDVIr = ((ds.ndvi - Fn) / (Fx - Fn)).clip(min=0, max=0.9)
    fPAR = (fPARmax * NDVIr).rename('fpar')
    inputs = xr.merge((LUE, fPAR))
    inputs.to_netcdf(path+'_LUE.nc', mode='w')
    return inputs

###
### Calling function
###


# alternate call function to run across all years of given site
# {'Big-Desert':h29v12, 'Black-Saturday':h29v12,
'Brindabella':h30v12, 'Deua-NP':h30v12, 'Howard-Springs':h30v10}
def multi_call(tile:str, meteor_site:str):

    d = {'Big-Desert':2001, 'Black-Saturday':2008,
'Brindabella':2002, 'Deua-NP':2001, 'Howard-Springs':2007}
    data_extent = 2017 ## EDITED

    for year in range(d[meteor_site],data_extent):
        global path
        path =
'/g/data/xc0/user/IvanK/thesis_data/outputs/{}_{}'.format(year,
meteor_site)
        print('Computing model for {} at
{}'.format(str(year),meteor_site))
        refl = get_reflectance(year,tile)
        call(year, tile, meteor_site, refl) # takes year to
process, MODIS tile name, and site name as in ANUCLIM data
    print('Outputs computed for all years at
{}'.format(meteor_site))


# call function for one year of MODIS data and modelling
def call(times: int, tile:str, site:str, data: xr.Dataset):

    co_mins = {'Big-Desert':(139.8548,-36.3545), 'Black-
Saturday':(144.9541,-37.8266), 'Brindabella':(148.1478,-36.0560),
'Deua-NP':(149.4392,-36.1984), 'Howard-Springs':(131.0318,-
12.6441)}
    co_maxs = {'Big-Desert':(142.7984,-34.3927), 'Black-
Saturday':(146.2319,-37.2262), 'Brindabella':(149.9033,-34.9068),
'Deua-NP':(150.1130,-35.5720), 'Howard-Springs':(131.3256,-
12.3915)}
    global min_lon, min_lat, max_lon, max_lat
    min_lon, min_lat = co_mins[site]
    max_lon, max_lat = co_maxs[site]

    data.drop(['red_630_690',
               'nir1_780_900',
               'blue_450_520',
               'green_530_610',
               'nir2_1230_1250',
               'swir1_1550_1750',
               'swir2_2090_2350',
               'ndvi_ok_mask',
               'ndii',
```

```
                'evir'])
    data.evi.to_netcdf(path+'_evi.nc')
    data.ndvi.to_netcdf(path+'_ndvi.nc')
    data.kc.to_netcdf(path+'_kc.nc')
    data.gvmi.to_netcdf(path+'_gvmi.nc')
    data.rmi.to_netcdf(path+'_rmi.nc')
    stamps = data.time

    call_gdalbash()
    subset_build_tif(stamps)

    fc = calculate_gcVI(times,site)
    fr = radiation_productivity(times,site)    # Calls zoom_data(),
subset_latlon() to process radiation data, and LUE_inputs() to
                                               # process NDVI and
EVI to fPAR and LUE respectively, and fday functions if used
    LUE_inputs()
    bash_rm_tif()

    msk = shape_mask(fr,site)
    GPP = xr.ufuncs.minimum(fc,fr).rename('GPP')
    GPP['fire_mask'] = msk
    GPP.to_netcdf(path+'_GPP_kc_final.nc')
    print('Computed model for {} at {}'.format(str(times),site))
    return
```